The ICF2 gene Zbtb24 specifically regulates the differentiation of B1 cells *via* promoting heme synthesis

Jun Wang[1*], He Gao[1], Sai Zhao[1], Xiao-Qiu Dai[1], Xiao-Yuan Qin[1], Wei-Long Zheng[1], Can Zhu[1], Hong-Min Wang[1], Xue-Mei Zhu[1], Fang-Yuan Gong[2], Xiao-Ming Gao[1*] and Ying Zhao[3*]

[1] Institutes of Biology and Medical Sciences, Suzhou Medical College of Soochow University, Suzhou 215123, China
[2] Department of Immunology, School of Biology and Basic Medical Sciences, Suzhou Medical College of Soochow University, Suzhou 215123, China
[3] Department of Pathophysiology, School of Biology and Basic Medical Sciences, Suzhou Medical College of Soochow University, Suzhou 215123, China

Corresponding authors:
Dr. Jun Wang and Dr. Xiao-Ming Gao, Institutes of Biology and Medical Sciences, Suzhou Medical College of Soochow University, 199 Ren-Ai Road, Suzhou Industrial Park, Suzhou 215123, Jiangsu Province, China. Tel/Fax: 86-512-65882135; Email: jwang79@suda.edu.cn or xmgao@suda.edu.cn

Dr. Ying Zhao, Department of Pathophysiology, School of Biology and Basic Medical Sciences, Suzhou Medical College of Soochow University, Suzhou 215123, China. Tel/Fax: 86-512-65880103; Email: yzhao@suda.edu.cn

ABSTRACT

Loss-of-function mutations of *ZBTB24* cause the Immunodeficiency, Centromeric Instability and Facial Anomalies syndrome 2 (ICF2). ICF2 is a rare autosomal recessive disorder with immunological defects in serum antibodies and circulating memory B cells, indicating an essential role of ZBTB24 in the terminal differentiation of B cells. Here we generated B-cell specific Zbtb24-deficient mice and systemically investigated its role in B cell development and function both *in vivo* and *in vitro*. Zbtb24 is dispensable for B cell development & maintenance in naive mice. Surprisingly, B-cell specific deletion of Zbtb24 does not evidently compromise germinal center reactions and the resulting primary & secondary antibody responses induced by T-cell dependent antigens, but significantly inhibits T-cell independent antigen-elicited antibody productions *in vivo*. At the cellular level, Zbtb24-deficiency specifically impedes the plasma cell differentiation of B1 cells without impairing their survival, activation and proliferation *in vitro*. Mechanistically, Zbtb24-ablation attenuates heme biosynthesis partially through mTORC1 in B1 cells, and addition of exogenous hemin abrogates the differentiation defects of Zbtb24-null B1 cells. Our study suggests that the defected B1 functions may contribute to recurrent infections in ICF2 patients, and discloses a B1-specific role of Zbtb24 in regulating plasma cell differentiation and antibody production, which is relevant for barrier defenses against invading pathogens.

Keywords: ICF2; Zbtb24; B1 cells; Plasma cell differentiation; Heme synthesis

INTRODUCTION

Immunodeficiency, centromeric instability and facial anomalies syndrome (ICF [OMIM 242860]) is a rare autosomal recessive and genetically heterogeneous disorder manifested with multiple system failures (Hu et al., 2019; Sterlin et al., 2016). Apart from the hypomethylated pericentromeric regions in specific chromosomes, and varying degrees of facial abnormalities & mental/motor defects, most ICF patients suffer from recurrent respiratory/gastrointestinal infections in early childhood owing to reduced antibody levels (Sterlin et al., 2016; Weemaes et al., 2013). Approximately 50% of ICF cases (ICF1) have mutations in the DNA methyltransferase 3B (*DNMT3B,* OMIM 602900), and about 30% of patients (ICF2) carry nonsense or missense mutations in the zinc finger and BTB domain containing 24 (*ZBTB24,* OMIM 614064) (de Greef et al., 2011; Weemaes et al., 2013; Xu et al., 1999). Although mutations in the cell division cycle associated 7 (*CDCA7*, OMIM 609937), helicase, lymphoid-specific (*HELLS*, OMIM 603946), and ubiquitin-like with plant homeodomain and ring finger domains 1 (*UHRF1*, OMIM 607990) have been recently shown to the associated with ICF3, ICF4 and an atypical ICF case, respectively, there are still few ICF cases (ICFX) left with unidentified disease genes (Thijssen et al., 2015; Unoki et al., 2023). In line with the similar molecular and clinical characteristics across different ICF subtypes, these disease genes act sequentially/corporately to modulate chromatin accessibilities and DNA methylations (Funabiki et al., 2023; Hardikar et al., 2020; Jenness et al., 2018; Ren et al., 2019; Thompson et al., 2018; Unoki et al., 2023; Wu et al., 2016).

Zbtb24 belongs to a large and evolutionary conserved family of transcriptional regulators with about 60 different members, many of which have prominent roles in hematopoietic development, differentiation and function (Cheng et al., 2021; Maeda, 2016; Zhu et al., 2018). For instance, Bcl6 (Zbtb27) promotes germinal center (GC) reactions by driving the differentiation of both GC B cells (GCB) and T follicular helper (Tfh) cells, and thereby is indispensable for the generation of high-affinity memory B cells (Bm) and long-lived antibody-secreting plasma cells (PCs) *in vivo* (Cheng et al., 2021; Toyama et al., 2002; Zhu et al., 2018). In addition, depletion of the ICF4 gene *Hells* in B cell compartment accelerates the premature decay of GCB cells and impairs the generation of high-affinity Bm and antibodies (Cousu et al., 2023). Thus, the absence of GC structures and circulating memory (but not total) B cells in *ZBTB24*-disrupted ICF2 patients indicate that ZBTB24

may possess similar functions in antibody responses *in vivo* (de Greef et al., 2011; Kloeckener-Gruissem et al., 2005; Weemaes et al., 2013; Zhu et al., 2018). Indeed, ZBTB24 modulates the function of human B lymphoblastoid cell line Raji by indirectly repressing Irf4 & Prdm1 in a Bcl6-independent manner (Liang et al., 2016). Moreover, ZBTB24 participates in the nonhomologous end joining process, and thereby promotes the class-switch recombination (CSR) in B cells either directly *via* binding to PARP1 or indirectly by inducing the expression of CDCA7 (Helfricht et al., 2020; Unoki et al., 2019). Nonetheless, the roles of Zbtb24 in the development/function of B cells and *in-vivo* antibody responses remain unknown.

As the effectors of humoral immunity, B cells are comprised of two populations, the predominant B2 subset and the minor B1 compartment (Montecino-Rodriguez and Dorshkind, 2006). B2 cells are continuously produced in the bone marrow (BM) from hematopoietic stem cells (HSCs) throughout life, and the newly formed B cells traffic to the spleen where they eventually mature into either follicular B (FOB) or marginal zone B (MZB) cells. By contrast, B1 cells are mainly seeded during fetal and early neonatal life, and the major population is maintained by self-renewal thereafter, although the adult BM may remain limited potential for B1 development (Baumgarth, 2011; Clarke et al., 2018). Upon activation by T-cell dependent antigens (TD-Ags), the conventional FOB cells enter the GC structure, where they undergo massive proliferation, somatic hypermutation (SHM) & CSR, and ultimately differentiate into Bm or PCs with the capacity to produce high-affinity antibodies (Victora and Nussenzweig, 2022). Conversely, MZB and B1 cells are innate-like B cells with limited B-cell receptor (BCR) repertoire, and are able to rapidly respond to T-cell independent antigens (TID-Ags)/self-antigens by secretion of natural antibodies (Aziz et al., 2015; Baumgarth, 2011; Clarke et al., 2018; Palm and Kleinau, 2021). They promptly and massively differentiate into mature PCs, and thereby provide antibody-mediated innate immune protection during microbial infections (Baumgarth, 2011; Genestier et al., 2007). Given that B1 cells normally reside in the pleura, peritoneum & intestines, they play an important role in barrier immunity to control microbes at mucosal surfaces. Apart from antimicrobial activities, natural antibodies, most of which are produced by B1 cells, help maintain tissue homeostasis by cross-reacting to epitopes expressed on dead/dying autologous cells (Aziz et al., 2015; Baumgarth, 2011; Clarke et al., 2018; Palm and Kleinau, 2021).

It has been well established that the function and fate of B cells are finely controlled by the

proper expressions of different transcription factors (TFs). Bcl6/Bach2/Pax5 maintains the phenotype of FOB cells, and promotes their proliferation, SHM and CSR in GC reactions, whereas Prdm1 and Xbp1 augment the differentiation of PCs. Irf4 regulates both of these processes as intermediate Irf4 induces Bcl6 and activation-induced cytidine deaminase (AID), which initiates SHM & CSR, while its high expression upregulates Prdm1 (Ochiai et al., 2013). In addition to the timely & spatially regulated expressions of these TFs, recent studies showed that metabolic reprogramming/adaptation shapes the differentiation & function of B cells as well (Boothby and Rickert, 2017; Foh et al., 2022; Jellusova, 2018). mTORC1 coordinates the increased anabolism and thus plays an essential role in the activation, proliferation and protein synthesis of cells that demand increased energy and building blocks (Boothby et al., 2022). PKC signaling dictates B cell fate by regulating the mitochondrial biogenesis/function partially through mTORC1 signaling (Tsui et al., 2018). Coinciding with their instant actions against pathogens, innate-like B1 and MZB cells exhibit augmented glucose/lipid uptake & metabolism as compared to FOB cells (Jellusova, 2018; Muri et al., 2019). Moreover, high mitochondrial reactive oxygen species (ROS) in activated B cells promotes CSR but dampens the generation of PCs *via* inhibiting the synthesis of heme, which inactivates Bach2 and thus releases its inhibition on Prdm1 expression and PC differentiation (Jang et al., 2015; Watanabe-Matsui et al., 2011).

As the germline deletion of Zbtb24 is embryonic lethal in mice (Wu et al., 2016), we herein generated B-cell specific Zbtb24 knockout mice (Zbtb24$^{B\text{-}CKO}$) to investigate its cell-intrinsic role in B cell development and function both *in vitro* and *in vivo*. Our data reveal that cell autonomous Zbtb24 is dispensable for the development/maintenance of B cells in naive mice and the TD-Ag-induced GC reactions and antibody responses, but greatly promotes the PC differentiation of peritoneal B1 cells *via* augmenting mTOCR1 activity and heme biosynthesis upon activation. Thus, our study not only suggests that the barrier defenses against pathogens might be impaired, owing to hampered differentiation of B1 cells, in respiratory & gastrointestinal tracts of ICF2 patients, but also provides mechanistic insights into the specific role of Zbtb24 in regulating B1 cell function.

159 # RESULTS

160 **Little effect of Zbtb24-deficiency on the development and phenotype of B cells in mice**

161 Given that the germline knockout of Zbtb24 is embryonic lethal in mice (Wu et al., 2016), we
162 generated mice harboring a conditional *Zbtb24*$^{loxp/+}$ allele with two loxp sites flanking the exon 2
163 which contains the translation starting site (**Figure 1A**). The N-terminal 316 amino acids, including
164 the BTB domain, the AT-hook domain and the first C_2H_2 Zinc finger motif, of Zbtb24 protein would
165 be specifically removed in Cre-expressing cells & tissues, which results in a frame shift in the
166 protein coding sequence and thereby generates a premature stop codon. To address cell-intrinsic
167 roles of Zbtb24 in the development and function of B cells *in vivo*, we crossed the *Zbtb24*$^{loxp/+}$ mice
168 with the *Cd19*-driven Cre-expressing mouse strain (*Cd19*$^{Cre/+}$) to generate B-cell specific Zbtb24
169 deficient (Zbtb24$^{B\text{-}CKO}$, *Cd19*$^{Cre/+}$*Zbtb24*$^{loxp/loxp}$) and the littermate control (Cd19$^{Cre/+}$,
170 *Cd19*$^{Cre/+}$*Zbtb24*$^{+/+}$) mice. Zbtb24$^{B\text{-}CKO}$ mice grew normally, and were phenotypically
171 indistinguishable from the control Cd19$^{Cre/+}$ mice.

172 In Zbtb24$^{B\text{-}CKO}$ mice, Zbtb24 was specifically and efficiently deleted from CD19-expressing
173 pre-B & pro-B cells onwards in the BM and peripheral B cells, while its expression in CD19-
174 negative BM pre-pro B cells, splenocytes and thymocytes were intact as analyzed by Q-PCR and/or
175 western blot (**Figure 1B-D**). Notably, lack of Zbtb24 affected neither the percentages/absolute
176 numbers of different developing stages of B cells in the BM (**Figure E**), nor the numbers of splenic
177 FOB/MZB cells as well as the peritoneal B2, B1a/B1b cells in the periphery (**Figure S1A&B**).
178 Moreover, the percentages of GCB in the spleens, mesenteric lymph nodes (MLN) & Peyer's
179 Patches (PP), and the serum total IgM, IgG & IgA levels were all normal in Zbtb24$^{B\text{-}CKO}$ mice
180 (**Figure S1C**, and **Figure 1F**). Thus, depletion of B-cell Zbtb24 has little impact on the early BM
181 B-cell development, the phenotype & maintenance of peripheral B cells, and serum antibody levels
182 in naive mice.

183 **Largely normal humoral responses to TD-Ags in Zbtb24$^{B\text{-}CKO}$ mice**

184 The major immunological features of ICF2 patients are hypogammaglobulinemia and lack of
185 circulating Bm cells, possibly owing to the disrupted germinal center reactions (Banday et al., 2020;
186 Kloeckener-Gruissem et al., 2005; Liang et al., 2016; Weemaes et al., 2013). We thus first
187 characterized TD-Ag-induced humoral responses in mice with B-cell specific Zbtb24 deficiency.

One week after immunization with NP_{19}-OVA (4-Hydroxy-3-nitrophenylacetyl hapten conjugated to ovalbumin) emulsified in IFA (incomplete Freund adjuvant, NP-OVA/IFA), serum levels of NP-specific IgM, IgG1 and IgG2c were significantly reduced in Zbtb24$^{B\text{-}CKO}$ mice. Surprisingly, on day 14 only NP-specific IgG2c was still slightly decreased, while the other two subtypes were reverted to normal levels in Zbtb24$^{B\text{-}CKO}$ mice (**Figure 2A&B**). Moreover, the percentages & numbers of CD19^{+}CD95^{high}CD38^{low} GCB as well as CD19^{low}CD138^{++} PC in spleens were all comparable between control and Zbtb24$^{B\text{-}CKO}$ mice (**Figure 2C&D**). Within gated GCB cells, percents of CD86^{low}CXCR4^{high} dark zone centroblasts and CD86^{high}CXCR4^{low} light zone centrocytes were comparable between the two genotypes of mice as well (**Figure 2C**). Consistent with our previous findings in human cells, lack of Zbtb24 did not affect the expressions of Bcl6, the key driving TF for GC reactions, in gated either GCB (defined as CD19^{+}CD95^{high}CD38^{low}) compartment or total CD19^{+} B cells (**Figure S2A&B**). In addition, the numbers of splenic GCB & PC cells were comparable in Cd19$^{Cre/+}$ & Zbtb24$^{B\text{-}CKO}$ mice immunized with sheep red blood cells (SRBC) as well (**Figure S2C**), further corroborating the dispensability of Zbtb24 on their differentiations *in vivo*. Notably, Zbtb24 was efficiently depleted in purified GCB cells (**Figure S2D**), thus it is unlikely that Zbtb24-expressing cells outcompete Zbtb24-null ones to fill the GCB compartment in TD-Ag-immunized Zbtb24$^{B\text{-}CKO}$ mice.

Given that the generation of specific antibodies appeared to be delayed in Zbtb24$^{B\text{-}CKO}$ mice upon immunization, we immunized mice with NP-OVA/IFA on day 0, and boosted the mice with the same antigen intraperitoneally once again on day 53 to further determine the impact of B-cell Zbtb24-deficiency on humoral responses elicited by TD-Ags *in vivo* (**Figure 2E**). Akin to previous results, control mice produced significantly more NP-specific IgG1 and IgG2c on day 10, and the differences went down greatly on day 20 post the primary immunization (**Figure 2F**). Of note, comparable levels of NP-specific antibodies were detected between the two groups thereafter, even on day 7 & 17 post the secondary challenge (**Figure 2F**). The numbers of PCs were normal in spleens of Zbtb24$^{B\text{-}CKO}$ as well (**Figure 2G)**.

We also immunized mice with a high dose of NP_{19}-OVA (100 μg/mouse) adsorbed on alum, which predisposes to the Th2 immune response instead of Th1 triggered by IFA *in vivo*. Again, reduced antigen-specific IgG1 were only observed early (day 7) post the primary immunization (**Figure S3A&B**). Moreover, specific deletion of Zbtb24 in B-cell compartment did not affect the

ratios of high-affinity to low-affinity (against NP_2-BSA & NP_{25}-BSA, respectively) IgG1 & IgG2c before (i.e., day 70) and two weeks (i.e., day 84) post the secondary immunization (**Figure S3C&D**). Given that Zbtb proteins may act redundantly to maintain the integrity and function of immune cells (Zhu et al., 2018), we conducted RNA-Seq analysis on purified splenic B cells before & after LPS stimulation to determine if any Zbtb proteins were evidently upregulated to compensate for the loss of Zbtb24. Levels of all Zbtb proteins, except Zbtb24, did not differ significantly between time-matched control and Zbtb24$^{B\text{-}CKO}$ splenic B cells (**Table S1**).

To exclude any potential off-target deletions of Zbtb24 in Zbtb24$^{B\text{-}CKO}$ mice, we next adoptively transferred purified splenic control or Zbtb24-deficient CD19^{+} B cells, together with WT CD4^{+} Th cells, into Rag2$^{-/-}$ recipients (**Figure S4A**). After immunization, serum levels of antigen-specific IgG, and total numbers of splenic CD19^{+} B cells or CD19^{low}CD138^{++} PCs did not differ in Rag2$^{-/-}$ recipients implanted with control *vs.* Zbtb24-dificient B cells (**Figure S4C-D**). Notably, the total serum IgM and IgG were reduced in Rag2$^{-/-}$ mice reconstituted with Zbtb24-depleted B cells (**Figure S4B**). Decreased total polyreactive IgM might underlie the reduced levels of NP-specific IgM in Zbtb24$^{B\text{-}CKO}$ mice (**Figure S4B&C**), as ablation of Zbtb24 did not profoundly affect the CSR ability of murine splenic B cells *in vitro* (**Figure S5**).

Collectively, these data indicate that B-cell intrinsic Zbtb24 does not play an essential role in the generation and maintenance of GCB cells, their affinity maturation as well as later differentiation toward Bm or PCs after immunization, albeit that Zbtb24$^{B\text{-}CKO}$ mice show delayed/mitigated early extrafollicular antibody productions induced by TD-Ag.

Significantly reduced humoral responses to TID-Ags in Zbtb24$^{B\text{-}CKO}$ mice

The reduced total serum IgM & IgG, most of which likely react against autoantigens and commensal gut bacteria, in Rag2$^{-/-}$ mice reconstituted with Zbtb24-deficient B cells indicate that lack of Zbtb24 hampers antibody responses elicited by TID-Ags (**Figure S4B**). Indeed, Zbtb24$^{B\text{-}CKO}$ mice produced significantly decreased amounts of NP-specific IgM, IgG1 and IgG3, three major antibody subtypes against soluble protein or carbohydrate antigens in mice (Zhao et al., 2022), in the first two weeks after immunization with the type II TID-Ag NP-Ficoll. On day 21 & 35, levels of IgG1 were still reduced, and the other two antibody subtypes tended to decrease as well (**Figure 3A**). Likewise, significantly less NP-specific IgM, IgG1, IgG3 and IgG2b were detected in male Zbtb24$^{B\text{-}CKO}$ mice after immunization with the type I TID-Ag NP-LPS (**Figure**

248 **3F**). As expected, reduced percentages/numbers of $CD19^{low}CD138^{++}$ PCs were detected in spleens
249 and/or peritoneal cavities (PeC) of $Zbtb24^{B\text{-}CKO}$ mice (**Figure 3B-E & G-H**).
250 B1 and MZB cells are considered the main responders to TID-Ags (Haas, 2011). We thus tried
251 to delineate which cell type was responsible for the diminished antibody levels in TID-Ag-
252 immunized $Zbt24^{B\text{-}CKO}$ mice *via* detailed flow cytometry analyses. Five weeks post NP-Ficoll
253 immunization, the numbers of NP-specific cells in differentially gated B-cell compartments were
254 all comparable in the spleens and PeC between $Cd19^{Cre/+}$ and $Zbtb24^{B\text{-}CKO}$ mice (**Figure S6**),
255 possibly due to the late analyzing time point. Of note, significantly less NP^{+} B1, but not FOB or
256 MZB, cells were observed in the spleens of $Zbtb24^{B\text{-}CKO}$ mice three weeks post NP-LPS inoculation,
257 and NP^{+} B1 cells tended to decrease in their PeC as well (**Figure S7**), indicating that B1 was the
258 target B-cell subset through which Zbtb24 promoted TID-Ag-induced antibody responses *in vivo*.
259 **Zbtb24-deficiency impairs the differentiation and antibody-producing ability of B1 cells *in***
260 ***vivo***
261 To unambiguously reveal the roles of Zbtb24 in B1 cells, we adoptively transferred peritoneal B1
262 cells, purified from $Cd19^{Cre/+}$ or $Zbtb24^{B\text{-}CKO}$ mice by FACS-sorting, into $Rag2^{-/-}$ mice with no
263 mature T/B cells and serum antibodies (**Figure 4A**). Total IgM levels were significantly lower in
264 $Rag2^{-/-}$ recipients received Zbtb24-deficient B1 cells (**Figure 4B**). Moreover, 7 days after NP-LPS
265 immunization (i.e., day 27 post transfer), Zbtb24-deficient B1-reconstituted $Rag2^{-/-}$ recipients
266 produced significantly less NP-specific IgM than those harboring control $Cd19^{Cre/+}$ B1 cells
267 (**Figure 4C**). Total or NP-specific IgG was hardly detectable in recipients implanted with Zbtb24-
268 deficient or sufficient B1 cells (data not shown).
269 Upon activation, some peritoneal B1 cells transit to the spleen to divide and differentiate into
270 PCs, while others stay and rapidly differentiate into PCs even without division (Yang et al., 2007).
271 We thus compared the number of B & PCs in the spleens and PeC of recipients. The percentages
272 of Zbtb24-deficient $CD19^{+}$ B cells and $CD138^{+}$ PCs were significantly reduced in spleens, while
273 only the latter was decreased in the PeC of recipients (**Figure 4D&E**).
274 In sum, our data (depicted in **Figures 3&4**, and **S6&7)** indicate that lack of Zbtb24 suppresses
275 the differentiation of B1 cells toward PCs and thereby reduces the antibody levels against TID-Ags
276 *in vivo*. Given that surface levels of CD11b, which couples with CD18 to form Mac-1/CR3 and
277 governs the migration of B1 cells from the PeC into the spleens (Franke et al., 2020; Yang et al.,

278 2007), and surface IgM were comparable on Zbtb24-deficient and -sufficient peritoneal B1 cells
279 (**Figure S8A&B**), it is unlikely that reduced PC differentiation was attributable to impaired
280 migration or BCR-triggering.

281 **Zbtb24-deficiency impedes the PC differentiation of B1 cells without compromising their**
282 **survival, activation and proliferation *in vitro***

283 Upon activation by LPS *in vitro*, the differentiation of purified peritoneal B1, but not B2, cells
284 towards $CD138^+$ PCs was significantly impaired by Zbtb24 depletion (**Figure 5A-C**). Accordingly,
285 levels of IgM & IgG3 in culture supernatants were reduced in LPS-cultivated Zbtb24-null B1 cells
286 (**Figure 5D**). Given that B1 cells are more sensitive to TLR agonists-induced PC differentiation
287 than FOB cells (Genestier et al., 2007), we further cultured splenic B cells with anti-IgM/CD40 or
288 high amounts of LPS to mimic the T-cell dependent or independent stimulations, respectively.
289 Again, deficiency of Zbtb24 did not suppress the PC differentiation of splenic B2 cells as well as
290 their antibody producing abilities in these conditions (**Figure S8C-E**), corroborating our *in vivo*
291 findings depicted in **Figures 2D&G** and **S4D**. Zbtb24-deficiency did not reduce the viabilities and
292 cell numbers in these B1/B2 cultures (**Figures 5C**, and **S9A, D&E**). Moreover, the ability of B1/B2
293 cells to upregulate surface activation makers (CD69 & CD86) were not impaired by Zbtb24
294 depletion, excluding a generally disrupted signaling transduction downstream of TLR4 in B cells
295 deprived of Zbtb24 (**Figure S9B, C&F**).

296 As reported previously (Sindhava and Bondada, 2012), B1 cells were anergic to BCR
297 triggering and thus failed to undergo activation upon anti-IgM stimulation *in vitro* (**Figure S9B,**
298 **C&F**). To further determine the role of Zbtb24 in cell proliferation, we labelled B1 cells with cell
299 division tracker CFSE before culture. Interestingly, LPS stimulation induced massive PC
300 differentiation accompanied by minimal cell divisions, whereas anti-CD40 elicited robust
301 proliferation concurrent with little CD138 upregulation (**Figure 5E**), implying that B1 cells were
302 able to uncouple PC differentiation from the cell division process. Of note, Zbtb24-depletion
303 significantly repressed PC differentiation of B1 cells without impeding their mitoses induced by
304 LPS or anti-CD40 *in vitro* (**Figure 5E**).

305 Based on these data, we conclude that Zbtb24 promotes the PC differentiation of B1 cells
306 independent of their survival, activation and proliferation *in vitro*.

307 **Zbtb24-deficiency inhibits the PC differentiation of B1 cells *via* attenuating heme synthesis**

We next performed RNA-Seq analysis to explore how Zbtb24 regulates the differentiation of B1 cells. Upon activation by LPS, Zbtb24-deficient peritoneal B1, but not splenic B2 cells, expressed significantly lower levels of hallmark genes involved in PC differentiation, UPR (unfolded protein response) and protein secretion, such as *Prdm1* (the driving force of PC differentiation), *Sd1* (encoding CD138), *Irf4* and *Xbp1* (**Figure 6A, B&D**, and **Table S1**). Of note, expressions of Bach2 & Bcl6, two major TFs repressing Prdm1, were not influenced by Zbtb24 depletion in B1 cells (**Figure 6B**). Therefore, it is unlikely that the B1-specific effect of Zbtb24 on PC differentiation is attributable to its direct binding and regulation of these key regulators.

Enormous studies recently showed that the activation and function of lymphocytes are intertwined with metabolic reprogramming & adaption (Boothby and Rickert, 2017; Foh et al., 2022; Jellusova, 2018). In association with the altered function, multiple genes relating to nutrients uptake and metabolism, such as Slc2a1/Glut1, Slc16a3/Mct3, Ak4, Pdk1, Pfkl, and Tpi, were significantly upregulated in Zbtb24$^{B\text{-}CKO}$ B1 cells (**Figure S10A**). Accordingly, GSEA identified a positive enrichment of gene sets regulating the glycolysis and pyruvate metabolism in Zbtb24-null B1 cells (**Figure S10C**). By contrast, a panel of genes involved in heme metabolism were downregulated in Zbtb24$^{B\text{-}CKO}$ cells (**Figures 6A&C**, and **S10B**), albeit that the differences did not reach the cutoff value. Expressions of Alad (5-aminolevulinic acid dehydratase) and Cpox (Coproporphyrinogen oxidase), two enzymes that directly catalyze reactions along the heme synthesis pathway in cytosol and mitochondrial intermembrane space, respectively (Ajioka et al., 2006), were consistently reduced in Zbtb24-null B1 but not B2 cells (**Figure 6C**, and **Table S1**). Moreover, the level of Hmox1, a heme-induced oxygenase that mediates its degradation and serves as a readout for intracellular heme content (Watanabe-Matsui et al., 2011), was mildly decreased in Zbtb24$^{B\text{-}CKO}$ B1 cells as well (**Figure 6C**). Given that heme promotes Prdm1 expression and PC differentiation of B cells by inactivating Bach2 (Watanabe-Matsui et al., 2011), we reasoned that heme biosynthesis may be attenuated in Zbtb24-depleted B1 cells, thereby leading to impaired PC differentiation.

Indeed, Zbtb24-depletion significantly mitigated LPS-induced upregulation of protoporphyrin IX (PPIX), the final substrate of heme biosynthesis (Ajioka et al., 2006), in B1 cells, albeit no differences were observed in resting cells (**Figure 6E**). Notably, ablation of Zbtb24 resulted in a more pronounced PPIX reduction in CD138^{-} non-PC cells than that in CD138^{+} PC cells (26.2% *vs.*

338 10.1%, **Figure 6E**). Moreover, addition of exogenous hemin in cultures almost completely
339 abrogated the differentiation defects of Zbtb24-deficient B1 cells (**Figure 7F&H**), while its
340 supplementation similarly promoted/suppressed PC differentiation/CSR in control *vs.* Zbtb24$^{B\text{-}CKO}$
341 splenic B cells (**Figure S11A&B)**. Together, these data indicate that Zbtb24 specifically promotes
342 the PC differentiation of B1 cells *via* augmenting heme synthesis. Exogenous hemin only slightly
343 potentiated the PC differentiation of control B1 cells (**Figure 7F&H**), implying that activated
344 peritoneal B1 cells may contain abundant intracellular heme to facilitate their accelerated and
345 heightened PC differentiation.

346 **Zbtb24-depletion represses the heme synthesis partially through mTORC1 in B1 cells**

347 It has been recently shown that endogenous ROS inhibits heme synthesis, and activated splenic B
348 cells with intermediate mitochondrial mass/membrane potential are predisposed to become PCs
349 (Jang et al., 2015). We thus wondered whether Zbtb24 promoted heme synthesis in B1 cells *via*
350 regulating intracellular ROS and mitochondrial function. Compared to activated splenic B cells,
351 B1 cells had significantly higher levels of ROS, which were further increased by Zbtb24-depletion
352 (**Figures 7F-I**, and **S11C&D**). However, addition of the antioxidant L-ascorbic acid (L-AC) failed
353 to promote PC differentiation in peritoneal B1 cells, albeit that it did reduce ROS levels in B1 cell
354 and augment the PC differentiation of splenic B2 cells (**Figures 7F-I**, and **S11A&B**). The
355 mitochondrial mass/membrane potential was markedly lower in splenic B2-derived PCs as
356 previously reported (Jang et al., 2015), but no such differences were observed in B1 cultures, and
357 no significant impact of Zbtb24-deficiency on mitochondrial mass/membrane potential of B cells
358 was observed (**Figures 7G&I**, and **S11C&D**). Thus, the metabolic reprogramming and
359 mitochondrial function differ significantly between B1 *vs.* B2 cells along their differentiation
360 toward PCs. Because ROS represses the final step of heme synthesis by inhibiting the addition of
361 ferrous ions to PPIX (Jang et al., 2015), it is unlikely that disturbed ROS levels were unlikely
362 responsible for the attenuated PPIX accumulation in Zbtb24-deficient B1 cells.

363 Expressions of Slc3a2 & Slc7a5, encoding the respective heavy & light chain of CD98,
364 positively correlate with mTORC1 activity in B cells (Tsui et al., 2018). RNA-Seq data showed
365 that levels of Slc3a2 & Slc7a5 were decreased, coinciding with the disturbed mTORC1 signaling
366 in activated Zbtb24-null B1 cells as revealed by GSEA (**Figure S10A&C**). mTORC1 activity
367 regulates the protein synthesis & metabolism of mammalian cells, and promotes PC differentiation

368 of murine splenic B cells partially *via* augmenting heme synthesis (Tsui et al., 2018). In keeping
369 with these findings obtained in B2 cells, inclusion of an mTORC1 specific antagonist, Rapamycin,
370 significantly suppressed the PC differentiation and PPIX levels in peritoneal B1 cells (**Figure**
371 **7A&B**), demonstrating that mTORC1 promotes heme synthesis and PC differentiation of B1 cells
372 as well. In line with this notion, Zbtb24-depletion significantly repressed the expression of
373 phosphorylated ribosomal protein S6 (p-S6), an event controlled by mTORC1 activity (Tsui et al.,
374 2018), in LPS-stimulated B1 cells (**Figure 7C&D**). Notably, the inhibition was more pronounced,
375 akin to PPIX contents, in $CD138^-$ cells as compared to that in $CD138^+$ PCs (**Figures 6E**, and
376 **7C&D**), indicating that the impaired mTORC1 activity underlie, at least partially, the attenuated
377 heme synthesis and PC differentiation of Zbtb24-null B1 cells.

378 We noticed that PC differentiation and intracellular PPIX levels were still considerably reduced
379 in mTORC1 repressed (i.e., cultured with LPS plus Rapamycin) Zbtb24-null B1 cells (**Figure**
380 **7A&B**). To determine the extent to which the two factors (mTORC1 activity *vs.* heme accumulation)
381 contribute to the defected PC differentiation of Zbtb24-deficient B1 cells, we differentiated B1
382 cells in the presence of Rapamycin/hemin alone or both (**Figure 7E&F**). Supplementation of hemin
383 not only completely reverted the defects caused by Zbtb24-depletion as previously observed in
384 **Figure 6F&H**, but also partially relieved the inhibitory effect of Rapamycin on PC differentiation
385 of B1 cells. Of note, control and Zbtb24-null B1 cells exhibited comparable PC differentiation in
386 the presence of both Rapamycin and hemin (**Figure 7E&F**), implying that attenuated intracellular
387 heme synthesis is mainly responsible for the differentiation defects of Zbtb24-deficient B1 cells.

388 Collectively, our data show that Zbtb24 promotes the PC differentiation of B1 cells mainly
389 through augmenting heme synthesis, and the attenuated heme biosynthesis in Zbtb24-depleted B1
390 cells is partially attributed to their impaired mTORC1 activity.

391 **No effect of Zbtb24-deficiency on PC differentiation of MZB cells**

392 Akin to B1 cells, MZB cells are specialized in responses to TID-Ags and more sensitive, compared
393 to conventional FOB cells, to TLR agonists-induced proliferation (**Figure 8A**) and PC
394 differentiation (Genestier et al., 2007). We thus questioned whether Zbtb24 exerts a similar function
395 in this innate-like B cell subset as well. LPS stimulation induced robust cell division and PC
396 differentiation of MZB cells, while BCR-crosslinking elicited massive proliferation accompanied
397 by mild PC generation (**Figure 8A-C**). Notably, neither the proliferation nor the PC differentiation

of LPS-cultivated MZB cells were affected by Zbtb24 depletion, and the addition of exogenous hemin enhanced PC differentiation of Zbtb24 deficient or sufficient MZB cells to the same extent (**Figure 8A-D**). Hence, depletion of Zbtb24 does not impact the PC differentiation of MZB cells.

Notably, in stark contrast to the massive PC differentiation but little proliferation of peritoneal B1 cells (**Figure 5E**), the vigorous LPS-elicited differentiation of MZB cells was companied by extensive cell division (**Figure 8A-C**). Moreover, depletion of Zbtb24 resulted in a subtle but nevertheless consistent decrease of divided $CFSE^{low}$ MZB cells in anti-IgM-stimulated cultures (**Figure 8A&B**). This slightly reduced BCR-elicited proliferations of MZB cells may contribute to the decreased antibody levels in $Zbtb24^{B\text{-}CKO}$ mice after TID-Ag immunization as well. We speculated that the distinct metabolic adaptation and energy/substrate allocation between proliferation and differentiation in B1 *vs.* MZB cells, triggered by different stimuli, might underlie the distinct effects of Zbtb24 in these cells.

DISCUSSION

The clinical and immunological presentations of *ZBTB24*-disrupted ICF2 patients imply a prominent role of ZBTB24 in the terminal differentiation and antibody secretion of human B lymphocytes *in vivo* (Banday et al., 2020; Weemaes et al., 2013). Thus, we here systemically characterized the cell autonomous role of Zbtb24 in B cell development, differentiation and function by using the conditional knockout mice. Unexpectedly, our data demonstrate that B-cell Zbtb24 is virtually dispensable for TD-Ag-induced GC reactions & antibody responses *in vivo*, but its deficiency specifically impeding the PC differentiation B1 cells and thereby reduces TID-Ags-induced antibody productions. Our study thus not only provides a plausible explanation for the recurrent respiratory and gastrointestinal infections in ICF2 patients, but also is relevant for B1 cell-mediated barrier defenses and immune regulations.

Despite the reduced levels of serum antibodies and peripheral $CD19^{+}CD27^{+}$ Bm cells, total amounts of circulating T and B lymphocytes are normal in most ICF cases (Banday et al., 2020; Weemaes et al., 2013). Moreover, detailed anatomical and immunological examinations revealed the absence of GC structure in one ICF2 patient devoid of Zbtb24, and downregulating its expression inhibits the proliferation of a human B cell line by indirectly repressing Prdm1 & Irf4 *in vitro* (Kloeckener-Gruissem et al., 2005; Liang et al., 2016; Weemaes et al., 2013). Given the essential role of GC in the propagation of Bm and antibody-secreting PCs (Victora and Nussenzweig, 2022), these findings strongly indicate that ZBTB24 controls *in-vivo* antibody responses through regulating the GC structure/reaction rather than the general development/maintenance of lymphocytes in humans. In partial agreement of this notion, specific deletion of Zbtb24 in B cell compartment from the $CD19^{+}$ pro-B stage onwards (*Cd19*-Cre) has no effect on the later development, maintenance and phenotype of B cells in the BM & periphery of mice. However, contrary to the Bm and antibody defects in *ZBTB24*-disrupted ICF2 patients, neither the GCB numbers, nor the primary/secondary antibody responses elicited by TD-Ags are significantly decreased in $Zbtb24^{B\text{-}CKO}$ mice, regardless of antigen doses and adjuvant types used for immunization. In keeping with these *in-vivo* findings, Zbtb24-depletion does not impair the *in-vitro* survival, activation, proliferation and differentiation of FOB cells, the main responders to TD-Ags. Furthermore, mice with a specific depletion of Zbtb24 in T cells (*Cd4*-Cre) or the whole hematopoietic lineages (*Vav*-Cre) exhibit normal B cell development and largely intact TD-Ag-

453 induced antibody responses *in vivo* as well (unpublished data).

454 Hence, hematopoietic Zbtb24 is dispensable for B cell development/maintenance and the
455 canonical TD-Ag-induced antibody responses *via* GC reactions in mice. The latter is clearly distinct
456 from *ZBTB24*-disrupted ICF2 patients with hypo- or a-gammaglobulinemia and lack of circulating
457 Bm cells (Banday et al., 2020; Weemaes et al., 2013). The discrepancies in (memory) humoral
458 responses between ICF2 patients and aforementioned Zbtb24-deficient mice may stem from the
459 distinct functions of Zbtb24 across species as evidenced by the fact that Zbtb24-null embryo is only
460 viable in humans but not in mice (Wu et al., 2016). It is also possible that Zbtb24 may regulate TD-
461 Ag-induced GC reaction and antibody responses beyond the hematopoietic system, for instance,
462 through supporting the formation of proper B cell follicular cell networks that steers the GC output
463 (Lutge et al., 2023). Nonetheless, a functional substitution of Zbtb24 by other Zbtb proteins, albeit
464 unlikely based on our RNA-Seq data in splenic B cells, could not be completely excluded.

465 By contrast, our data highlight an important role of B-cell Zbtb24 in humoral responses against
466 TID-Ags *in vivo.* Upon immunization with a type I or type II TID-Ag, Zbtb24$^{B\text{-}CKO}$ mice generate
467 significantly less antibody-secreting PCs in the presence of normal amounts of B1, FOB and MZB
468 cells. At the cellular level, depletion of Zbtb24 markedly restrains the ability of B1 cells to
469 differentiate into PCs and produce antibodies both *in vitro* upon LPS stimulation and *in vivo* after
470 transfer into Rag2$^{-/-}$ recipients without impairing their *in-vitro* survival, activation and proliferation.
471 MZB cells are the other main responders, beyond B1 cells, to TID-Ags, and these two innate-like
472 B cell subsets behave similarly in many aspects. For example, both B1 and MZB are hypersensitive
473 to TLR agonists-induced PC differentiation (Genestier et al., 2007). Strikingly, Zbtb24-ablation
474 does not markedly impact the proliferation & PC differentiation of MZB cells. Therefore, our study
475 discloses that B1 cells are the main target B-cell subset through which Zbtb24 augments TID-Ag-
476 elicited antibody productions in *vivo*.

477 Unlike conventional FOB cells that need to undergo extensive proliferation before terminal
478 differentiation, B1 cells do no respond readily to BCR-induced clonal expansion, possibly owing
479 to the highly expressed inhibitory co-receptors like CD5 & Lyn. Instead, B1 cells secrete natural
480 IgM at steady state in the absence of antigenic stimulation, and upon encountering with non-
481 specific inflammatory/pathogen-associated stimuli, they promptly and vigorously differentiate into
482 antibody (mainly IgM)-secreting cells (Genestier et al., 2007; Holodick and Rothstein, 2013;

483 Sindhava and Bondada, 2012). These polyreactive IgM not only participates in the maintenance of
484 tissue homeostasis and prevention of autoimmune reactions, but also constitutes an important first-
485 line defense against infections before the activation of adaptive immune system by facilitating the
486 clearance of autologous dead/dying cells or invading pathogens, respectively (Morris et al., 2019).
487 Moreover, B1 cells may regulate the immune response independent of antibody secretion. Both at
488 steady state and after activation, B1 cells may function as a sort of regulatory B (Breg) cells by
489 producing copious amounts of anti-inflammatory cytokine IL-10 (Catalan et al., 2021). Zbtb24-
490 deficeint B1 cells produce less IgM and IL-10, it is thus tempting to speculate that the dysfunctional
491 B1 cells contribute to the commonly-occurred infections as well as the uncommonly-observed
492 autoimmune manifestations in ICF2 patients (Banday et al., 2020), albeit that the putative surface
493 markers defining human B1 cells remain controversial so far (Sanz et al., 2019).

494 The promptly upregulated PC differentiation and antibody-producing ability of B1 cells upon
495 activation imply that they are transcriptionally and metabolically well prepared for the high
496 secretory capacity. Indeed, innate-like B1 and MZB cells constitutively express more Prdm1 while
497 less Bcl6, and are bioenergetically more active than conventional FOB cells (Genestier et al., 2007;
498 Jellusova, 2018). Moreover, sustained mTORC1 signaling coordinates an immediate UPR-
499 affiliated transcriptome profile preceding the expression of Xbp1, and confers MZB cells the ability
500 to undergo rapid and robust PC differentiation even in the presence of cell cycle inhibitors
501 (Gaudette et al., 2020; Gaudette et al., 2021), which mirrors the unique mitosis-independent PC
502 differentiation of B1 cells as we showed here. In activated conventional splenic B cells, mTORC1
503 promotes heme synthesis partially by reducing intracellular ROS, and thereby augments their PC
504 differentiation because heme induces Prdm1 by inactivating its repressor molecule Bach2 (Jang et
505 al., 2015; Tsui et al., 2018; Watanabe-Matsui et al., 2011). Once synthesized, heme enhances
506 mTORC1 activity, possibly through Prdm1 induction or modulating the mitochondrial function
507 (Price et al., 2021; Tsui et al., 2018). We here showed that mTORC1 exerts a similar function in B1
508 cells as Rapamycin-mediated mTORC1 inhibition greatly inhibits the PC differentiation and heme
509 accumulation in B1 cells as well. Given that Zbtb24-depletion reduces mTORC1 activity and PPIX
510 content, and that hemin supplementation almost completely reverts the differentiation defects of
511 Zbtb24-null B1 cells even in the presence of Rapamycin, our data reveal that Zbtb24 promotes the
512 PC differentiation of B1 cells mainly *via* heme synthesis, which is partially mediated through

513 mTORC1. Detailed mechanisms underlying the regulations of mTORC1 activity and heme
514 synthesis in B1 cells by Zbtb24 merit further investigation.

515 Both human and murine Bm cells possess an enhanced heme signature than naive B cells, and
516 supplementation of hemin promotes their differentiation towards PCs (Price et al., 2021). Thus,
517 increased heme biosynthesis seems to be a conserved feature of B cells with accelerated &
518 augmented PC differentiation potential, including B1, MZB & Bm cells. The comparable antibody
519 levels between control and Zbtb24$^{B\text{-}CKO}$ mice after secondary TD-Ag challenge indicate that
520 Zbtb24 has little effect on heme metabolism and PC differentiation of murine Bm cells. Why
521 Zbtb24 only influences the heme biosynthesis and PC differentiation of B1, but not other B cells,
522 at least in mice, is intriguing. Although MZB and B1 cells are considered innate-like B cells and
523 able to mount rapid antibody responses against invading pathogens before the adaptive immune
524 responses are properly propagated and matured, these two cell types are functionally distinct at
525 many aspects. For instance, our data demonstrate that only B1 cells are able to largely uncouple
526 PC differentiation from cell division upon activation, albeit that MZB cells may differentiate into
527 PCs in the presence of cell cycle blockers (Gaudette et al., 2021). It is thus conceivable that B1
528 cells, depending on the types of stimulation (i.e., LPS *vs.* anti-CD40 triggering), adopt distinct
529 metabolic pathways to devote most of the anergy & biomolecule building blocks either to the PC
530 differentiation/antibody secretion pathway or to the mitosis process. We hypothesize that in case of
531 the PC differentiation pathway, B1 cells immensely and sharply elevate heme biosynthesis, and
532 Zbtb24 somehow participates in this metabolic adaptation process partially by regulating mTORC1
533 activity. In MZB cells, this metabolic reprogramming is much milder and thus less affected by
534 Zbtb24 deficiency. Despite that mice deficient in *Hmox1*, the heme degrading enzyme, have
535 increased serum antibody levels, administration of hemin to mice does not augment antibody
536 responses against TD- or TID-Ags (Kapturczak et al., 2004; Price et al., 2021; Watanabe-Matsui et
537 al., 2011), indicating a complex effect of heme *in vivo*.

538 During the preparation of this manuscript, Chen's group reported that ablation of Zbtb24 in B
539 cell compartment (*Cd19*-Cre) had no effect on basal serum antibody levels and TD-Ag-induced
540 GC reactions in mice as well (Ying et al., 2023), corroborating our findings in this aspect. They
541 found that Zbtb24-depletion upregulated Il5ra expression, which results in augmented CD19
542 activity and impaired MZB proliferation induced by BCR (Ying et al., 2023). In partial agreement

with their findings, BCR-triggered proliferation of MZB cells were impaired upon Zbtb24-depletion, albeit that the defect was far milder in our hands. Moreover, our RNA-Seq analysis in splenic B cells did not reveal any differences in Il5ra expression. These discrepancies may relate to different strategies used to generate the conditional knockout mice. Nonetheless, we here extend the role of Zbtb24 in humoral immune response by showing that lack of Zbtb24 significantly impedes the mTORC1 activity, heme synthesis and PC differentiation of B1 cells, leading to diminished TID-Ag-induced antibody productions *in vivo*. Thus, Zbtb24 may represent an important factor involved in regulating barrier defenses against pathogens through B1 cells.

567 # MATERIALS AND METHODS

568 **Mice**

569 The *Zbtb24* conditional allele (*Zbtb24*$^{loxp/+}$) was generated using the CRISPER/Cas9 strategy
570 (Beijing CasGene Biotech. Co., Ltd). Briefly, C57BL/6 embryonic stem cells (ES) were transfected
571 with the targeting vectors *via* electroporation. Correctly targeted clones, containing two loxp sites
572 inserted into the flanking regions of *Zbtb24* exon 2 with the translation starting site (**Figure 1A**),
573 were identified by PCR and injected into blastocytes to generate chimeric mice. Chimeric mice
574 were then crossed with C57BL/6 wild type (WT) mice to obtain F1 mice with the germline-
575 transmitted *Zbtb24*$^{loxp/+}$ allele. After multiple-step crossing the heterozygous *Zbtb24*$^{loxp/+}$ mouse
576 with Cd19$^{Cre/+}$ mouse on a C57BL/6 background (kindly provided by Prof. Biao Zheng, East China
577 Normal University), mice with the specific deletion of *Zbtb24* in CD19^{+} B cells (Zbtb24$^{B\text{-}CKO}$,
578 *Cd19*$^{Cre/+}$*Zbtb24*$^{loxp/loxp}$) were generated. Primers used for ES clone selection and genotyping were
579 listed in **Table S2**. To exclude the impact of *Cd19*-driven Cre expression on B cells (Zhao et al.,
580 2022), littermate *Cd19*$^{Cre/+}$*Zbtb24*$^{+/+}$ (Cd19$^{Cre/+}$) mice were used as controls in all the analysis
581 unless otherwise indicated. Immunodeficient *Rag2*$^{-/-}$ C57BL/6 mice with no mature T & B cells
582 (Changzhou Cavens Laboratory Animal Co., Ltd) were used as recipients in adoptive transfer
583 experiments. Mice were housed under specific pathogen-free (SPF) conditions and all experiments
584 were performed in accordance with procedures approved by the Ethics Committee of Soochow
585 University.

586 **Immunizations**

587 Mice were immunized with the TD-Ag NP_{19}-OVA emulsified in IFA (Sigma, 1:1) or adsorbed onto
588 Imject Alum (Thermo Scientific, 1:1), or with the TID-Ag NP-AECM-Ficoll (NP-Ficoll)/NP-LPS
589 intraperitoneally. NP_{19}-OVA, NP-Ficoll and NP-LPS were all obtained from Biosearch
590 Technologies.

591 **B-cell Isolation and Culture**

592 BM cells were harvested by flushing the femurs of mouse, and peritoneal cells were isolated by
593 lavaging the PeC with 10 ml PBS. Splenocytes were obtained by mechanically dissociating spleens
594 in PBS, followed by passing through a 70 μM nylon mesh (BD Biosciences). Erythrocytes were
595 removed by addition of ammonium chloride lysis buffer. Total CD19^{+} B, CD19^{+}CD23^{high}CD21^{low}

596 FOB and $CD19^{+}CD23^{low}CD21^{high}$ MZB cells in spleens, or peritoneal $CD19^{+}B220^{low}CD23^{-}$ B1
597 and $CD19^{+}B220^{high}CD23^{+}$ B2 cells were sorted out *via* a FACS Aria cell sorter III (BD Biosciences)
598 with > 95% purity. MojoSort™ Mouse Pan B Cell Isolation Kit II (Biolegend) were used to enrich
599 $CD19^{+}$ B cells in splenocytes before sorting.

600 Purified B cells were cultured in medium, LPS (L2630, Sigma), goat $F(ab')_2$ anti-mouse IgM
601 (αIgM, SouthernBiotech) or rat anti-mouse CD40 (αCD40, 1C10, Biolegend) in the
602 absence/presence of recombinant mouse IL-4, human TGF-β1 and B-cell activating factor (BAFF)
603 (all from Peprotech) in 96 U-bottom plates at 37°C for indicated times. The complete culture
604 medium was RPMI-1640 (Hyclone) supplemented with non-essential amino acids (Sigma), 10%
605 heat-inactivated fetal bovine serum (FBS, Gibco), 100 U/ml penicillin (Beyotime), 100 μg/ml
606 streptomycin (Beyotime), 50 μM β-mercaptoethanol (Sigma), 1 mM sodium pyruvate and 10 mM
607 HEPES (Hyclone). In some cases, L-ascorbic acid (L-AC, #A92902, Sigma), hemin (#9039,
608 Sigma), Rapamycin (Absin), and corresponding vehicle controls were added at indicated
609 concentrations from the beginning of culture.

610 **Adoptive Transfer Experiments**

611 $CD4^{+}$ T cells were isolated with MojoSort™ Mouse CD4 T cell isolation kit (Biolegend) from
612 spleens of WT mice with > 90% purity. Purified splenic $CD19^{+}$ B cells, from $Cd19^{Cre/+}$ or $Zbtb24^{B-}$
613 ^{CKO} mice, were mixed with $CD4^{+}$ T cells at the ratio of 2:1 before being injected into $Rag2^{-/-}$
614 recipients *via* the tail vein (5 x 10^6 B cells plus 2.5 x 10^6 $CD4^{+}$ T cells/200 μl PBS/mouse). One
615 day later, recipient mice were immunized with NP_{19}-OVA emulsified in IFA. To analyze the
616 function of B1 cells *in vivo*, FACS-sorted peritoneal B1 cells were injected into $Rag2^{-/-}$ recipients
617 intraperitoneally (2 x 10^5 cells/200 μl PBS/mouse) followed by NP-LPS immunization.

618 **ELISA**

619 Mouse sera or B-cell culture supernatants were collected at indicated time points and immediately
620 stored at -20°C until the analysis for antibody levels by ELISA. In brief, ELISA plates (Nunc) were
621 coated with goat anti-mouse Ig (SouthernBiotech, 1010-01, 1:1000) or NP_{25}-BSA (Biosearch
622 Technologies, 5 μg/ml) to capture all murine Igs or NP-specific antibodies, respectively. After
623 washing with PBS containing 0.05% Tween-20, wells were blocked with PBS containing 3% BSA
624 before incubation with diluted sera or culture supernatants. The optimal dilutions for each Ig
625 subtype were determined by preliminary experiments. Total or NP-specific IgM, IgG1, IgG2b,

626 IgG2c, IgG3 and IgA levels were detected by using HRP-coupled goat anti-mouse subtype-specific
627 secondary antibodies (SouthernBiotech).

628 **Western Blot and Q-PCR Analysis**

629 Cells were lysed for 1 hr on ice in RIPA lysis buffer (Beyotime) supplemented with protease and
630 phosphatase inhibitors (Selleck). Proteins were separated in an SDS-PAGE 10% gel and
631 subsequently blotted onto a PVDF membrane (Millipore). After incubation with blocking buffer
632 (Tris-buffered saline with 5% nonfat milk), the membrane was incubated with primary antibodies
633 overnight at 4°C, followed by a further incubation with secondary antibodies at room temperature
634 (RT) for 2 hrs. Signals were visualized with the Tanon 3500 Gel Imaging System (Tanon). The
635 following antibodies were used: anti-Zbtb24 (PM085, MBL Life Science, 1:1000), anti-Gapdh
636 (AF0006, Beyotime, 1:1000), HRP-coupled donkey anti-Guinea pig (H+L, 706-035-148, Jackson
637 ImmunoResearch Lab) and HRP-conjugated horse anti-mouse IgG (7076S, CST).

638 Total RNA was extracted from indicated cells by the Total RNA Kit II (OMEGA). cDNA was
639 subsequently synthesized using Reverse Transcriptase M-MLV (TakaRa) according to
640 manufacturer's instructions. mRNA levels of indicated genes were quantitatively determined by
641 SYBR-green technology on an ABI-StepOnePlus Sequence Detection System (Applied
642 Biosystems). Sequence of primers used for RT-qPCR analysis were listed in **Table S2**.

643 **Flow Cytometric Analysis**

644 Single cell suspensions were prepared and surface molecules were stained at 4°C for 30 mins with
645 optimal dilutions of each antibody. The following antibodies were used: anti-mouse B220 (RA3-
646 6B2), CD45 (30-F11), CD19 (6D5), CD23 (B3B4), CD5 (53-7.3), CD38 (90), CXCR4 (L276F12),
647 CD69 (H1.2F3), CD86 (PO3), IgG1 (RMG1-1) and IgG2b (RMG2b-1) (all from Biolegend); anti-
648 mouse CD21/35 (eBio4E3 or eBio8D9), CD43 (eBioR2/60), CD93 (AA4.1) and IgM (II/41) (all
649 from eBioscience); and anti-mouse CD138 (281-2), CD95 (Jo2) and IgG3 (R40-82) (all from BD
650 Biosciences). Sometimes 7-AAD (Biolegend) and NP-Ficoll-FITC (NP-FITC, Biosearch
651 Technologies) were additionally used to visualize NP-specific B cells as previously reported (Zhao
652 et al., 2022). After staining, cells were washed twice with PBS, suspended in 300 μl PBS, and fixed
653 volumes of cells were processed with the Attune® NxT Acoustic Focusing Cytometer (Thermo
654 Scientific). Data were analyzed by FlowJo software (BD Biosciences).

655 To measure the mitochondrial membrane potential and intracellular ROS, cells were incubated

656 in pre-warmed RPMI-1640 containing MitoTracker^{TM} Orange CMTMRos (Thermo Scientific, 50
657 nM) and DCFH-DA (Beyotime, 5 μM) at 37°C for 30 mins. After extensive washing, cells were
658 further stained with antibodies against surface molecules as indicated above.

659 For intracellular detection of TFs, cells were fixed/permeabilized with Foxp3 staining buffer
660 set (eBioscience) before incubation with antibodies against BCL6 (7D1), PRDM1 (5E7) and IRF4
661 (IRF4.3E4) (all from Biolegend). To measure mTORC1 activity, cells were fixed with 4%
662 paraformaldehyde, permeabilized by ice-cold methanol for 30 mins on ice, and then stained with
663 the primary antibody recognizing phosphor-S6 ribosomal protein (Ser235/236) (D57.2.E, CST),
664 followed by incubating with the secondary APC-coupled AffinityPure F(ab')2 Fragment Donkey
665 anti-Rabbit IgG antibody (711-606-152, Jackson Immunolab).

666 **RNA-sequencing and analysis**

667 Total cellular RNA was extracted with the Total RNA Kit II (OMEGA). Library construction and
668 sequencing was performed on a HiSeq or Novaseq 2x150 platform by AZENTA Life Sciences
669 (Suzhou). Sequenced reads were mapped to reference murine genome (mm10 assembly) using
670 bowtie2 with default parameters, and Cufflinks was used to estimate the abundance of transcripts
671 (Langmead and Salzberg, 2012; Trapnell et al., 2010). Quantifications of gene expression were
672 performed using RSEM, and the expression levels of genes in each sample were normalized by
673 means of fragments per kilobase of transcript per million mapped reads (FPKM). These RNA-seq
674 data were deposited in the GEO database with the accession number GSE241746 & GSE241747.

675 After eliminating absent features (zero counts), differential expressed genes (DEGs) between
676 two groups with 2-3 replicates (one mouse per replicate) were compared *via* DEseq2. Genes were
677 considered to be differentially expressed with the cutoff of fold change ≥ 0.414 and P value < 0.05.
678 To identify signaling pathways enriched in different samples, we used R package clusterProfiler
679 and software Gene Set Enrichment Analysis (GSEA) of MSigDB gene sets (Hallmark, KEGG, and
680 GO) (Subramanian et al., 2005; Yu et al., 2012). GSEA was performed for each pairwise
681 comparison using gene lists ranked by the Wald statistic.

682 **PPIX measurement**

683 Levels of PPIX in cells were analyzed by flow cytometry with excitation at 405 nm and emission
684 at 610/20 nm as described previously (Jang et al., 2015; Tsui et al., 2018).

685 **Statistical Analysis**

The GraphPad Prism 8.0 software (GraphPad) was used to generate graphs and perform statistical analysis. Data were expressed as mean ± SEM. An unpaired nonparametric Mann-Whitney test was utilized to compare differences among groups unless otherwise indicated. Values at $P < 0.05$ were considered significant.

DATA AVAILABILITY

The RNA-Seq data were deposited in the GEO database with the accession number GSE241746 (review token: uxebqggyvjwfdaj) & GSE241747 (review token: krmbyuiwbtwzpwv). The majority of data supporting the findings of this study are presented within the article and its Supplemental Material. Data that are not directly included are available from the corresponding author upon reasonable request.

FOOTNOTES

Acknowledgements: This study was financially supported by the National Natural Science Foundation of China (32170914/81970371/31670888 & 81470564); and Priority Academic Program Development of Jiangsu Higher Education Institutions (PAPD).

Author contributions: JW conceived and coordinated the study; JW, HG, SZ, XYQ, ZWL, CZ and YZ performed the experiments; JW, HG, SZ and XYQ analyzed the data; XQD conducted bioinformatic analyses and generated relevant figures; HMW, FYG and XMZ assisted in flow cytometry analysis/sorting; JW and YZ drafted the manuscript; JW, XMG and YZ revised the manuscript and secured financial support.

Conflict of Interest: The authors declare no conflict of interest.

Materials & Correspondence: material request should be addressed to Dr Jun Wang, jwang79@suda.edu.cn

REFERENCES

Ajioka, R.S., Phillips, J.D., and Kushner, J.P. (2006). Biosynthesis of heme in mammals. Biochim Biophys Acta *1763*, 723-736.

Aziz, M., Holodick, N.E., Rothstein, T.L., and Wang, P. (2015). The role of B-1 cells in inflammation. Immunol Res *63*, 153-166.

Banday, A.Z., Jindal, A.K., Kaur, A., Kumar, Y., Nameirakpam, J., Patra, P.K., and Rawat, A. (2020). A young girl with hypogammaglobulinemia and granulomatous hepatitis caused by a novel mutation in ZBTB24 gene: A case based analysis. Immunobiology *225*, 151912.

Baumgarth, N. (2011). The double life of a B-1 cell: self-reactivity selects for protective effector functions. Nat Rev Immunol *11*, 34-46.

Boothby, M., and Rickert, R.C. (2017). Metabolic Regulation of the Immune Humoral Response. Immunity *46*, 743-755.

Boothby, M.R., Brookens, S.K., Raybuck, A.L., and Cho, S.H. (2022). Supplying the trip to antibody production-nutrients, signaling, and the programming of cellular metabolism in the mature B lineage. Cell Mol Immunol *19*, 352-369.

Catalan, D., Mansilla, M.A., Ferrier, A., Soto, L., Oleinika, K., Aguillon, J.C., and Aravena, O. (2021). Immunosuppressive Mechanisms of Regulatory B Cells. Front Immunol *12*, 611795.

Cheng, Z.Y., He, T.T., Gao, X.M., Zhao, Y., and Wang, J. (2021). ZBTB Transcription Factors: Key Regulators of the Development, Differentiation and Effector Function of T Cells. Front Immunol *12*, 713294.

Clarke, A.J., Riffelmacher, T., Braas, D., Cornall, R.J., and Simon, A.K. (2018). B1a B cells require autophagy for metabolic homeostasis and self-renewal. J Exp Med *215*, 399-413.

Cousu, C., Mulot, E., De Smet, A., Formichetti, S., Lecoeuche, D., Ren, J., Muegge, K., Boulard, M., Weill, J.C., Reynaud, C.A., and Storck, S. (2023). Germinal center output is sustained by HELLS-dependent DNA-methylation-maintenance in B cells. Nat Commun *14*, 5695.

de Greef, J.C., Wang, J., Balog, J., den Dunnen, J.T., Frants, R.R., Straasheijm, K.R., Aytekin, C., van der Burg, M., Duprez, L., Ferster, A.*, et al.* (2011). Mutations in ZBTB24 are associated with immunodeficiency, centromeric instability, and facial anomalies syndrome type 2. Am J Hum Genet *88*, 796-804.

Foh, B., Buhre, J.S., Sina, C., and Ehlers, M. (2022). Influence of nutrients and metabolites on the differentiation of plasma cells and implications for autoimmunity. Front Immunol *13*, 1004644.

Franke, K., Pillai, S.Y., Hoogenboezem, M., Gijbels, M.J.J., Matlung, H.L., Geissler, J., Olsman, H., Pottgens, C., van Gorp, P.J., Ozsvar-Kozma, M.*, et al.* (2020). SIRPalpha on Mouse B1 Cells Restricts Lymphoid Tissue Migration and Natural Antibody Production. Front Immunol *11*, 570963.

Funabiki, H., Wassing, I.E., Jia, Q., Luo, J.D., and Carroll, T. (2023). Coevolution of the CDCA7-HELLS ICF-related nucleosome remodeling complex and DNA methyltransferases. Elife *12*.

Gaudette, B.T., Jones, D.D., Bortnick, A., Argon, Y., and Allman, D. (2020). mTORC1 coordinates an immediate unfolded protein response-related transcriptome in activated B cells preceding antibody secretion. Nat Commun *11*, 723.

Gaudette, B.T., Roman, C.J., Ochoa, T.A., Gomez Atria, D., Jones, D.D., Siebel, C.W., Maillard, I., and Allman, D. (2021). Resting innate-like B cells leverage sustained Notch2/mTORC1 signaling to achieve rapid and mitosis-independent plasma cell differentiation. J Clin Invest *131*.

Genestier, L., Taillardet, M., Mondiere, P., Gheit, H., Bella, C., and Defrance, T. (2007). TLR agonists selectively promote terminal plasma cell differentiation of B cell subsets specialized in thymus-independent responses. J Immunol *178*, 7779-7786.

Haas, K.M. (2011). Programmed cell death 1 suppresses B-1b cell expansion and long-lived IgG production in response to T cell-independent type 2 antigens. J Immunol *187*, 5183-5195.

762 Hardikar, S., Ying, Z., Zeng, Y., Zhao, H., Liu, B., Veland, N., McBride, K., Cheng, X., and Chen, T. (2020). The
763 ZBTB24-CDCA7 axis regulates HELLS enrichment at centromeric satellite repeats to facilitate DNA methylation.
764 Protein Cell *11*, 214-218.
765 Helfricht, A., Thijssen, P.E., Rother, M.B., Shah, R.G., Du, L., Takada, S., Rogier, M., Moritz, J., H, I.J., Stoepker, C.,
766 *et al.* (2020). Loss of ZBTB24 impairs nonhomologous end-joining and class-switch recombination in patients
767 with ICF syndrome. J Exp Med *217*.
768 Holodick, N.E., and Rothstein, T.L. (2013). Atypical Response of B-1 Cells to BCR Ligation: A Speculative Model.
769 Front Immunol *4*, 457.
770 Hu, H., Chen, C., Shi, S., Li, B., and Duan, S. (2019). The gene mutations and subtelomeric DNA methylation in
771 immunodeficiency, centromeric instability and facial anomalies syndrome. Autoimmunity *52*, 192-198.
772 Jang, K.J., Mano, H., Aoki, K., Hayashi, T., Muto, A., Nambu, Y., Takahashi, K., Itoh, K., Taketani, S., Nutt, S.L., *et*
773 *al.* (2015). Mitochondrial function provides instructive signals for activation-induced B-cell fates. Nat Commun
774 *6*, 6750.
775 Jellusova, J. (2018). Cross-talk between signal transduction and metabolism in B cells. Immunol Lett *201*, 1-13.
776 Jenness, C., Giunta, S., Muller, M.M., Kimura, H., Muir, T.W., and Funabiki, H. (2018). HELLS and CDCA7 comprise
777 a bipartite nucleosome remodeling complex defective in ICF syndrome. Proc Natl Acad Sci U S A *115*, E876-
778 E885.
779 Kapturczak, M.H., Wasserfall, C., Brusko, T., Campbell-Thompson, M., Ellis, T.M., Atkinson, M.A., and Agarwal, A.
780 (2004). Heme oxygenase-1 modulates early inflammatory responses: evidence from the heme oxygenase-1-
781 deficient mouse. Am J Pathol *165*, 1045-1053.
782 Kloeckener-Gruissem, B., Betts, D.R., Zankl, A., Berger, W., and Gungor, T. (2005). A new and a reclassified ICF
783 patient without mutations in DNMT3B and its interacting proteins SUMO-1 and UBC9. Am J Med Genet A *136*,
784 31-37.
785 Langmead, B., and Salzberg, S.L. (2012). Fast gapped-read alignment with Bowtie 2. Nat Methods *9*, 357-359.
786 Liang, J., Yan, R., Chen, G., Feng, J., Wu, W.W., Ren, W., Zhu, C., Zhao, Y., Gao, X.M., and Wang, J. (2016).
787 Downregulation of ZBTB24 hampers the G0/1- to S-phase cell-cycle transition via upregulating the expression
788 of IRF-4 in human B cells. Genes Immun *17*, 276-282.
789 Lutge, M., De Martin, A., Gil-Cruz, C., Perez-Shibayama, C., Stanossek, Y., Onder, L., Cheng, H.W., Kurz, L.,
790 Cadosch, N., Soneson, C., *et al.* (2023). Conserved stromal-immune cell circuits secure B cell homeostasis and
791 function. Nat Immunol *24*, 1149-1160.
792 Maeda, T. (2016). Regulation of hematopoietic development by ZBTB transcription factors. Int J Hematol *104*,
793 310-323.
794 Montecino-Rodriguez, E., and Dorshkind, K. (2006). New perspectives in B-1 B cell development and function.
795 Trends Immunol *27*, 428-433.
796 Morris, G., Puri, B.K., Olive, L., Carvalho, A.F., Berk, M., and Maes, M. (2019). Emerging role of innate B1 cells in
797 the pathophysiology of autoimmune and neuroimmune diseases: Association with inflammation, oxidative and
798 nitrosative stress and autoimmune responses. Pharmacol Res *148*, 104408.
799 Muri, J., Thut, H., Bornkamm, G.W., and Kopf, M. (2019). B1 and Marginal Zone B Cells but Not Follicular B2
800 Cells Require Gpx4 to Prevent Lipid Peroxidation and Ferroptosis. Cell Rep *29*, 2731-2744 e2734.
801 Ochiai, K., Maienschein-Cline, M., Simonetti, G., Chen, J., Rosenthal, R., Brink, R., Chong, A.S., Klein, U., Dinner,
802 A.R., Singh, H., and Sciammas, R. (2013). Transcriptional regulation of germinal center B and plasma cell fates
803 by dynamical control of IRF4. Immunity *38*, 918-929.
804 Palm, A.E., and Kleinau, S. (2021). Marginal zone B cells: From housekeeping function to autoimmunity? J
805 Autoimmun *119*, 102627.
806 Price, M.J., Scharer, C.D., Kania, A.K., Randall, T.D., and Boss, J.M. (2021). Conserved Epigenetic Programming

807 and Enhanced Heme Metabolism Drive Memory B Cell Reactivation. J Immunol *206*, 1493-1504.
808 Ren, R., Hardikar, S., Horton, J.R., Lu, Y., Zeng, Y., Singh, A.K., Lin, K., Coletta, L.D., Shen, J., Lin Kong, C.S.*, et al.*
809 (2019). Structural basis of specific DNA binding by the transcription factor ZBTB24. Nucleic Acids Res *47*, 8388-
810 8398.
811 Sanz, I., Wei, C., Jenks, S.A., Cashman, K.S., Tipton, C., Woodruff, M.C., Hom, J., and Lee, F.E. (2019). Challenges
812 and Opportunities for Consistent Classification of Human B Cell and Plasma Cell Populations. Front Immunol
813 *10*, 2458.
814 Sindhava, V.J., and Bondada, S. (2012). Multiple regulatory mechanisms control B-1 B cell activation. Front
815 Immunol *3*, 372.
816 Sterlin, D., Velasco, G., Moshous, D., Touzot, F., Mahlaoui, N., Fischer, A., Suarez, F., Francastel, C., and Picard,
817 C. (2016). Genetic, Cellular and Clinical Features of ICF Syndrome: a French National Survey. J Clin Immunol *36*,
818 149-159.
819 Subramanian, A., Tamayo, P., Mootha, V.K., Mukherjee, S., Ebert, B.L., Gillette, M.A., Paulovich, A., Pomeroy, S.L.,
820 Golub, T.R., Lander, E.S., and Mesirov, J.P. (2005). Gene set enrichment analysis: a knowledge-based approach
821 for interpreting genome-wide expression profiles. Proc Natl Acad Sci U S A *102*, 15545-15550.
822 Thijssen, P.E., Ito, Y., Grillo, G., Wang, J., Velasco, G., Nitta, H., Unoki, M., Yoshihara, M., Suyama, M., Sun, Y.*, et*
823 *al.* (2015). Mutations in CDCA7 and HELLS cause immunodeficiency-centromeric instability-facial anomalies
824 syndrome. Nat Commun *6*, 7870.
825 Thompson, J.J., Kaur, R., Sosa, C.P., Lee, J.H., Kashiwagi, K., Zhou, D., and Robertson, K.D. (2018). ZBTB24 is a
826 transcriptional regulator that coordinates with DNMT3B to control DNA methylation. Nucleic Acids Res *46*,
827 10034-10051.
828 Toyama, H., Okada, S., Hatano, M., Takahashi, Y., Takeda, N., Ichii, H., Takemori, T., Kuroda, Y., and Tokuhisa, T.
829 (2002). Memory B cells without somatic hypermutation are generated from Bcl6-deficient B cells. Immunity *17*,
830 329-339.
831 Trapnell, C., Williams, B.A., Pertea, G., Mortazavi, A., Kwan, G., van Baren, M.J., Salzberg, S.L., Wold, B.J., and
832 Pachter, L. (2010). Transcript assembly and quantification by RNA-Seq reveals unannotated transcripts and
833 isoform switching during cell differentiation. Nat Biotechnol *28*, 511-515.
834 Tsui, C., Martinez-Martin, N., Gaya, M., Maldonado, P., Llorian, M., Legrave, N.M., Rossi, M., MacRae, J.I.,
835 Cameron, A.J., Parker, P.J.*, et al.* (2018). Protein Kinase C-beta Dictates B Cell Fate by Regulating Mitochondrial
836 Remodeling, Metabolic Reprogramming, and Heme Biosynthesis. Immunity *48*, 1144-1159 e1145.
837 Unoki, M., Funabiki, H., Velasco, G., Francastel, C., and Sasaki, H. (2019). CDCA7 and HELLS mutations undermine
838 nonhomologous end joining in centromeric instability syndrome. J Clin Invest *129*, 78-92.
839 Unoki, M., Velasco, G., Kori, S., Arita, K., Daigaku, Y., Yeung, W.K.A., Fujimoto, A., Ohashi, H., Kubota, T., Miyake,
840 K., and Sasaki, H. (2023). Novel compound heterozygous mutations in UHRF1 are associated with atypical
841 immunodeficiency, centromeric instability and facial anomalies syndrome with distinctive genome-wide DNA
842 hypomethylation. Hum Mol Genet *32*, 1439-1456.
843 Victora, G.D., and Nussenzweig, M.C. (2022). Germinal Centers. Annu Rev Immunol *40*, 413-442.
844 Watanabe-Matsui, M., Muto, A., Matsui, T., Itoh-Nakadai, A., Nakajima, O., Murayama, K., Yamamoto, M., Ikeda-
845 Saito, M., and Igarashi, K. (2011). Heme regulates B-cell differentiation, antibody class switch, and heme
846 oxygenase-1 expression in B cells as a ligand of Bach2. Blood *117*, 5438-5448.
847 Weemaes, C.M., van Tol, M.J., Wang, J., van Ostaijen-ten Dam, M.M., van Eggermond, M.C., Thijssen, P.E.,
848 Aytekin, C., Brunetti-Pierri, N., van der Burg, M., Graham Davies, E.*, et al.* (2013). Heterogeneous clinical
849 presentation in ICF syndrome: correlation with underlying gene defects. Eur J Hum Genet *21*, 1219-1225.
850 Wu, H., Thijssen, P.E., de Klerk, E., Vonk, K.K., Wang, J., den Hamer, B., Aytekin, C., van der Maarel, S.M., and
851 Daxinger, L. (2016). Converging disease genes in ICF syndrome: ZBTB24 controls expression of CDCA7 in

852 mammals. Hum Mol Genet *25*, 4041-4051.
853 Xu, G.L., Bestor, T.H., Bourc'his, D., Hsieh, C.L., Tommerup, N., Bugge, M., Hulten, M., Qu, X., Russo, J.J., and
854 Viegas-Pequignot, E. (1999). Chromosome instability and immunodeficiency syndrome caused by mutations in
855 a DNA methyltransferase gene. Nature *402*, 187-191.
856 Yang, Y., Tung, J.W., Ghosn, E.E., and Herzenberg, L.A. (2007). Division and differentiation of natural antibody-
857 producing cells in mouse spleen. Proc Natl Acad Sci U S A *104*, 4542-4546.
858 Ying, Z., Hardikar, S., Plummer, J.B., Hamidi, T., Liu, B., Chen, Y., Shen, J., Mu, Y., McBride, K.M., and Chen, T.
859 (2023). Enhanced CD19 activity in B cells contributes to immunodeficiency in mice deficient in the ICF syndrome
860 gene Zbtb24. Cell Mol Immunol *20*, 1487-1498.
861 Yu, G., Wang, L.G., Han, Y., and He, Q.Y. (2012). clusterProfiler: an R package for comparing biological themes
862 among gene clusters. OMICS *16*, 284-287.
863 Zhao, Y., Zhao, S., Qin, X.Y., He, T.T., Hu, M.M., Gong, Z., Wang, H.M., Gong, F.Y., Gao, X.M., and Wang, J. (2022).
864 Altered Phenotype and Enhanced Antibody-Producing Ability of Peripheral B Cells in Mice with Cd19-Driven
865 Cre Expression. Cells *11*, 700.
866 Zhu, C., Chen, G., Zhao, Y., Gao, X.M., and Wang, J. (2018). Regulation of the Development and Function of B
867 Cells by ZBTB Transcription Factors. Front Immunol *9*, 580.
868

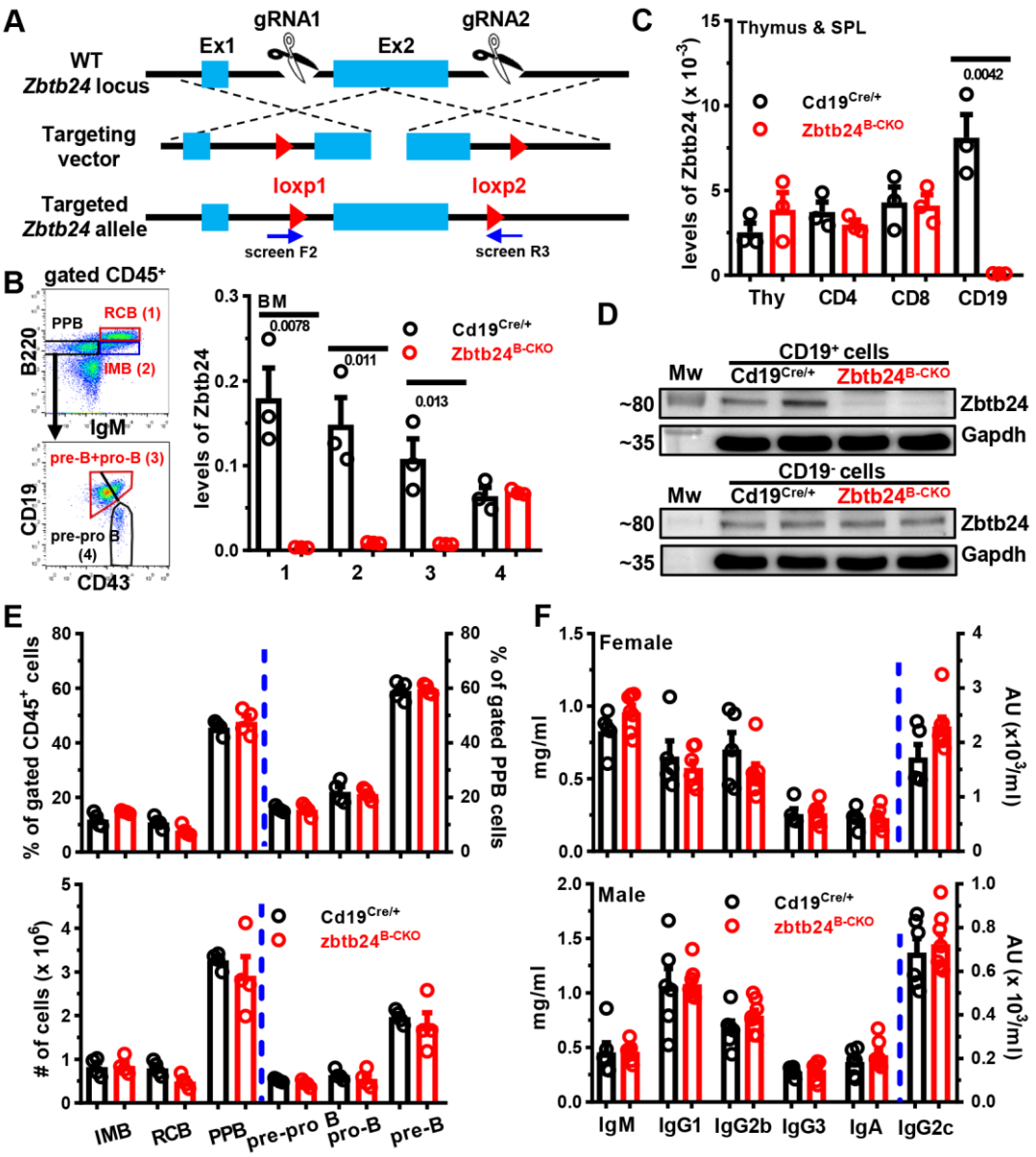

Figure 1. No effect of B-cell specific depletion of Zbtb24 on B-cell development in the bone marrow (BM) and baseline serum antibody levels in mice. A, a schematic representation for generating *Zbtb24*$^{loxp/+}$ mice using the CRISPER/CAS9 strategy. Screen F2 and R3 denote primers used to select correctly-targeted ES clones. **B-D**, efficient and specific deletions of Zbtb24 in CD19^{+} B cells in Cd19$^{Cre/+}$Zbtb24$^{loxp/loxp}$ (Zbtb24^{B-CKO}) mice. Levels of Zbtb24 were analyzed in FACS-sorted B220^{++}IgM^{+} recirculating mature B cells (RCB, gate 1), B220^{+}IgM^{+} immature B cells (IMB, gate 2), B220^{+}IgM^{-}CD19^{+}CD43^{-} pre-B plus B220^{+}IgM^{-}CD19^{+}CD43^{+} pro-B cells (gate 3), and B220^{+}IgM^{-}CD19^{-}CD43^{+} pre-pro B cells (gate 4) in the BM (**B**), or FACS-purified CD4^{+} (CD4), CD8^{+} (CD8) T cells and CD19^{+} (CD19) B cells in spleens (SPL) as well as total thymocytes (Thy) (**C**) of control Cd19$^{Cre/+}$ *vs.* Zbtb24^{B-CKO} mice by quantitative PCR. Sorting strategies for indicated BM B-cell subsets were shown in the left panel of **B**. Expressions of Zbtb24 were normalized to internal Gapdh (**B&C**). Protein levels of Zbtb24 were analyzed in beads-purified splenic CD19^{+} B cells (*upper panel*) and the remaining CD19^{-} fraction (*lower panel*) by Western blot (**D**). **E**, bar graphs showing the percents (*upper panel*) or absolute numbers (*lower panel*) of indicated B-cell subsets in the BM of control Cd19$^{Cre/+}$ and Zbtb24^{B-CKO} mice. **F**, bar graphs showing levels of total IgM, IgG1, IgG2b, IgG2c, IgG3 and IgA in sera of female (8-10 weeks old) and male (9-11 weeks old) Cd19$^{Cre/+}$ *vs.* Zbtb24^{B-CKO} mice. Each symbol/lane represents a single mouse of the indicated genotype, and numbers below horizonal lines indicate *P* values determined by student *t*-test (**B&C**). PPB, pre-pro/pro/pre B cells; Mw: molecular weight marker; AU, arbitrary units.

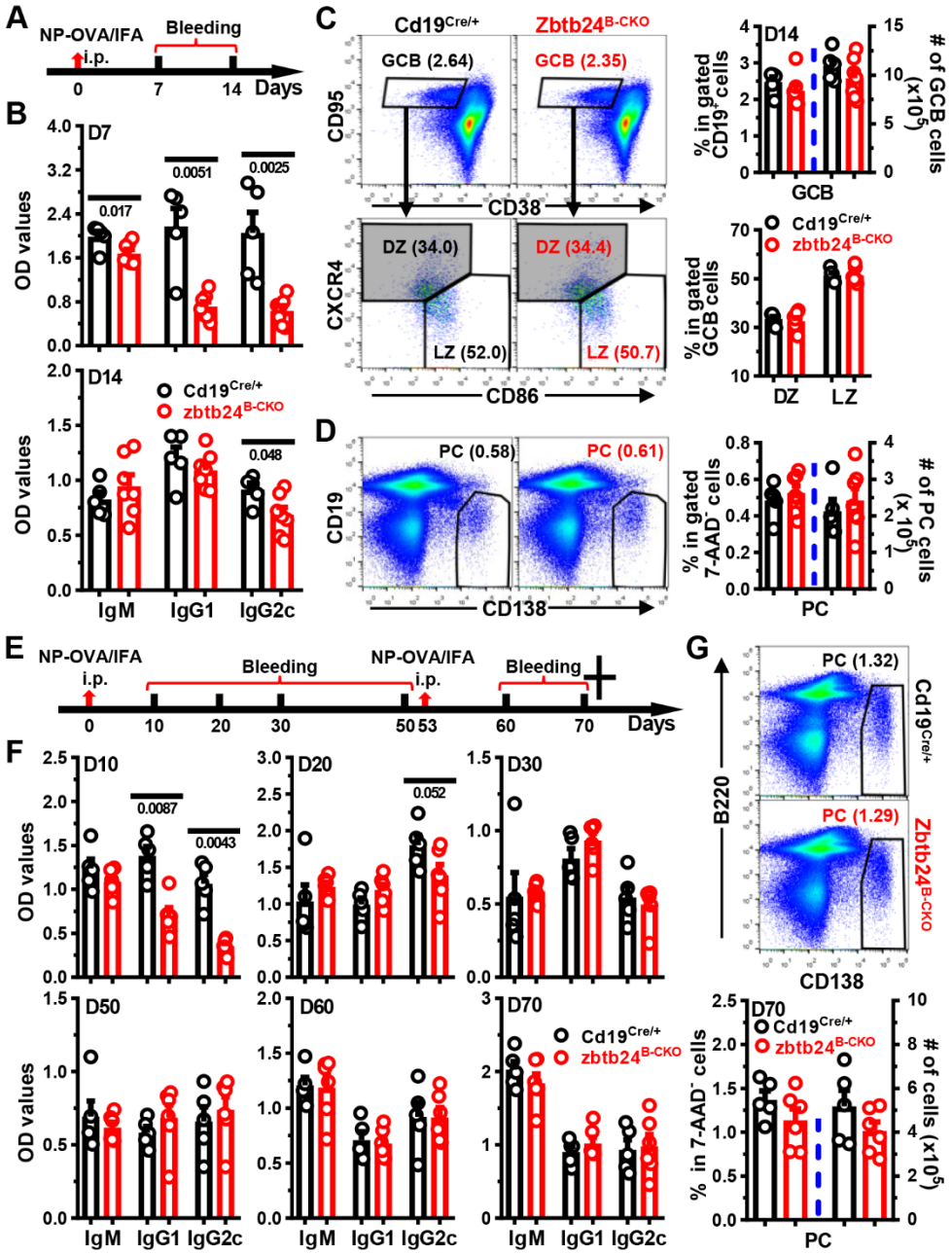

Figure 2. No significant defects in antibody responses in Zbtb24$^{B\text{-}CKO}$ mice post primary/secondary NP-OVA/IFA immunization. Mice (10-week old males in **A-D**; and 8-week old females in **E-G**) were intraperitoneally (i.p.) immunized with NP_{19}-OVA emulsified in IFA (1:1, 50 µg/100 µl/mouse) on D0, followed by i.p. rechallenging with NP_{19}-OVA/IFA (3:1, 20 µg/100 µl/mouse) on D53 (only in **E-G**). Sera were collected on indicated days and NP-specific antibodies were detected by ELISA. Cells in spleens on D14 (**C&D**) or D70 (**G**) were stained with antibodies, in combination with 7-AAD to exclude dead cells, to visualize the percents of CD19^{+}CD38^{low}CD95^{high} germinal center B (GCB) cells or CD19$^{-/low}$CD138^{high} plasma cells (PC) by flow cytometry. **A&E**, schematic diagrams illustrating the immunization and bleeding schedules of mice. **B&F**, bar graphs showing the optical density (OD) values of NP-specific antibodies in sera of Cd19$^{Cre/+}$ and Zbtb24$^{B\text{-}CKO}$ mice on indicated days. **C,** representative pseudo-plots showing the percentages of GCB (within gated 7-AAD^{-}CD19^{+} B cells) and frequencies of dark zone centroblasts (DZ, CXCR4^{high}CD86^{low}) and light zone centrocytes (LZ, CXCR4^{low}CD86^{high}) within gated GCB cells in control Cd19$^{Cre/+}$ and Zbtb24$^{B\text{-}CKO}$ mice. **D&G**, representative pseudo-plots showing the percentages of PCs in spleens of mice on D14 (**D**) or D70 (**G**). Cumulative data on the percentages or absolute numbers of indicated B-cell subsets were shown in the right of **C&D** or bottom of **G**. Each symbol represents a single mouse of the indicated genotype, and numbers below horizonal lines indicate *P* values while those in brackets denote percentages.

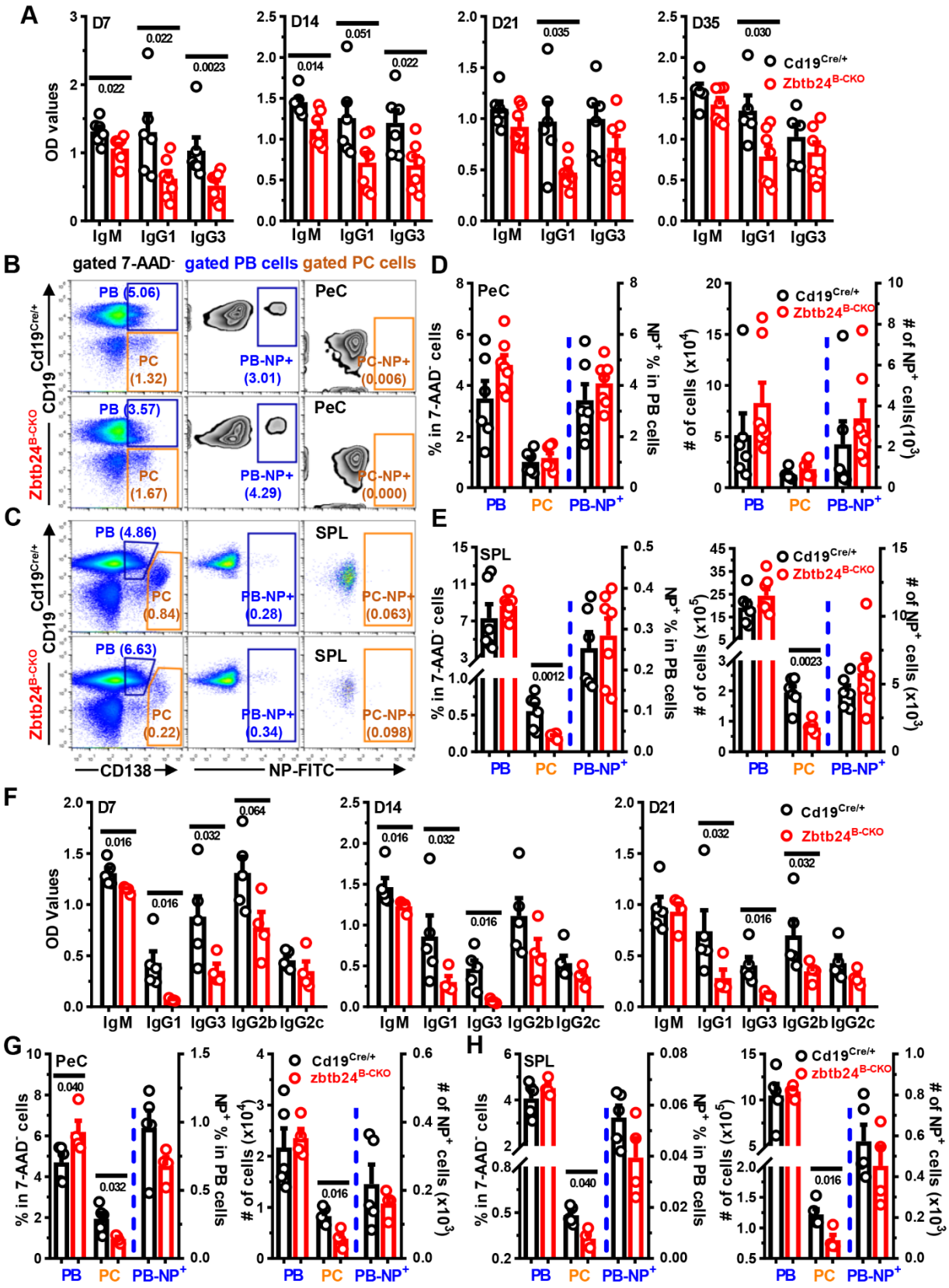

Figure 3. Significantly reduced antigen-specific antibody levels in Zbtb24$^{B\text{-}CKO}$ mice after TID-Ag immunization. Mice were intraperitoneally immunized with the type II TID-Ag NP-Ficoll (10 µg/200 µl PBS/mouse, **A-E**) or type I TID-Ag NP-LPS (20 µg/200 µl PBS/mouse, **F-H**) on D0. Blood was taken at indicated times and NP-specific antibodies in sera were determined by ELISA in plates coated with NP_{25}-BSA. **A&F**, bar graphs showing the optical density (OD) values of NP-specific antibodies in diluted sera of Cd19$^{Cre/+}$ *vs.* Zbtb24$^{B\text{-}CKO}$ mice on indicated days post immunization with NP-Ficoll (**A**) or NP-LPS (**F**). **B&C**, representative pseudo/zebra-plots illustrating the gating strategies for CD19^{+}CD138^{+} plasma blasts (PB)/CD19^{low}CD138^{high} plasma cells (PC) and percents of NP^{+} cells within gated PB (PB-NP^{+}) & PC (PC-NP^{+}) cells in peritoneal cavities (PeC, **B**) or spleens (SPL, **C**) of mice on D35 post NP-Ficoll immunization. **D&E and G&H**, bar graphs showing the percentages & absolute numbers of PB & PC cells as well as the NP^{+} cells within gated PB/PC cells (PB-NP^{+}/PC-NP^{+}, respectively) in PeC (**D&G**) and SPL (**E&H**) of mice on D35

post NP-Ficoll (**D&E**) or on D21 post NP-LPS (**G&H**) immunization. Each symbol represents a single mouse of the indicated genotype (female, 10 weeks of age in **A-E**; and male, 9 weeks of age in **F-H**), and numbers below horizonal lines in bar graphs indicate *P* values.

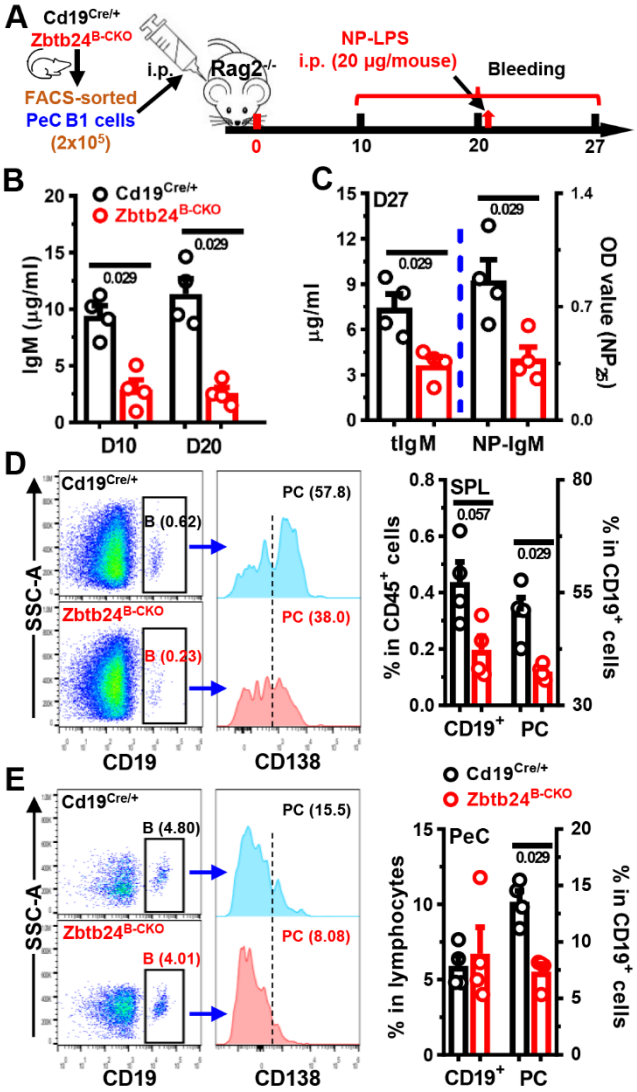

Figure 4. Impaired function of Zbtb24-deficient B1 cells *in vivo*. FACS-sorted peritoneal cavity CD19^{+}B220^{low}CD23^{-} B1 cells from control Cd19$^{Cre/+}$ and Zbtb24$^{B\text{-}CKO}$ mice (female, 12 weeks of age) were adoptively transferred into Rag2$^{-/-}$ recipient mice (female, 8 weeks of age) intraperitoneally (2x10^{5} cells/200 µl PBS/mouse). On D20 post injection, Rag2$^{-/-}$ recipient mice were immunized with NP-LPS (20 µg/200 µl PBS/mouse) intraperitoneally. Blood was taken at indicated times and cells in peritoneal cavities (PeC) & spleens (SPL) were analyzed by flow cytometry on D27. **A**, a schematic flow-chart showing the experiment setup. **B&C**, bar graphs showing levels of total (**B,** and tIgM in **C)** & NP-specific (NP-IgM in **C)** IgM in sera of recipient mice on D10 & D20 (**B**) or D27 (**C**). **D&E**, representative offset histograms/bar graphs showing the percentages of CD19+ B cells & CD19^{+}CD138^{+} plasma cells (PC) within gated B cells in the spleens (SPL, **D**) and peritoneal cavities (PeC, **E**) of recipients implanted with Cd19$^{Cre/+}$ or Zbtb24$^{B\text{-}CKO}$ B1 cells. Each dot represents a single recipient mouse, and numbers below horizontal lines indicate *P* values.

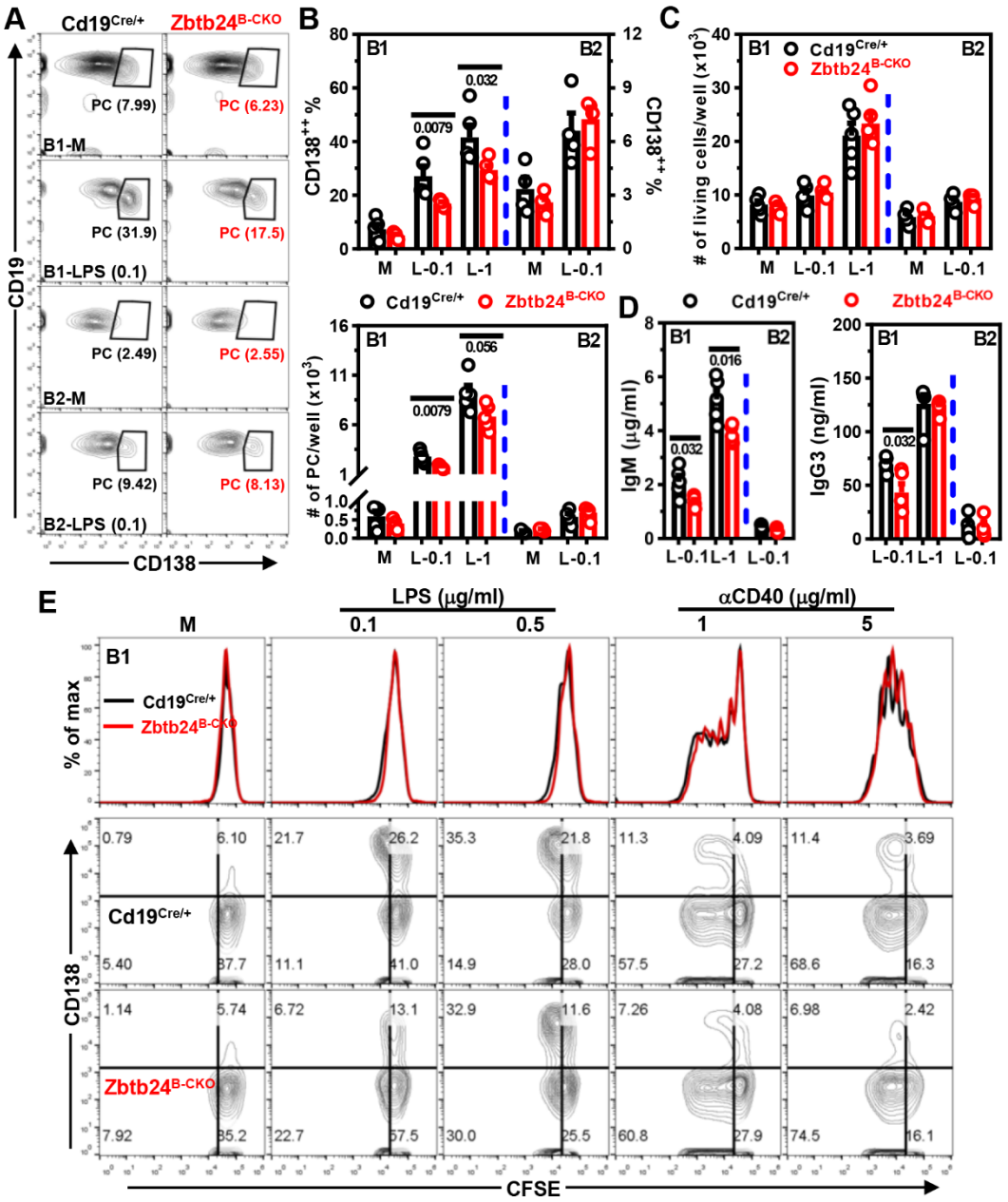

Figure 5. Zbtb24-deficiency specifically inhibits LPS-induced differentiation of peritoneal B1 cells toward PCs *in vitro*. CD19^{+}B220^{low}CD23^{-} B1 and CD19^{+}B220^{high}CD23^{+} B2 cells were FACS-sorted from peritoneal cavities of Cd19$^{Cre/+}$ & Zbtb24^{B-CKO} mice, and subsequently cultured (2-5 x 10^{4} cells/well in 96-U bottom plate) in medium (M), 0.1/1 μg/ml LPS (L-0.1/L-1, respectively) for 3 days. **A**, representative contour-plots showing the percentages of CD19^{low}CD138^{+} PCs in differentially cultured B1 or B2 cells on day 3. **B&C**, bar graphs showing the percentages/absolute numbers of PCs (**B**) or total living cells (**C**) 3 days post stimulation. **D**, bar graphs showing the IgM and IgG3 levels in culture supernatants of LPS-stimulated B1 or B2 cells on day 3. Antibody levels in supernatants of B cells cultured in medium were too low to be detected after 5x dilution. Each dot represents a single mouse of the indicated genotype (male, 10 weeks of age). **E**, representative overlayed histograms showing the comparable division profiles (*top panel*) or contour-plots showing the proliferation (CFSE) *vs.* differentiation (CD138, *middle and bottom panels*) of cultured peritoneal B1 cells isolated from Cd19$^{Cre/+}$ *vs.* Zbtb24^{B-CKO} mice (male, 14 weeks old, n=3/4 for Cd19$^{Cre/+}$ and Zbtb24^{B-CKO}, respectively). B1 cells were labelled with the cell division tracker CFSE (10 μM) and subsequently cultured in medium (M), LPS (0.1/0.5 μg/ml) or anti-IgM (αCD40, 1/5 μg/ml) for 3 days before flow cytometry analysis. Numbers below horizontal lines in **B-D** indicate *P* values.

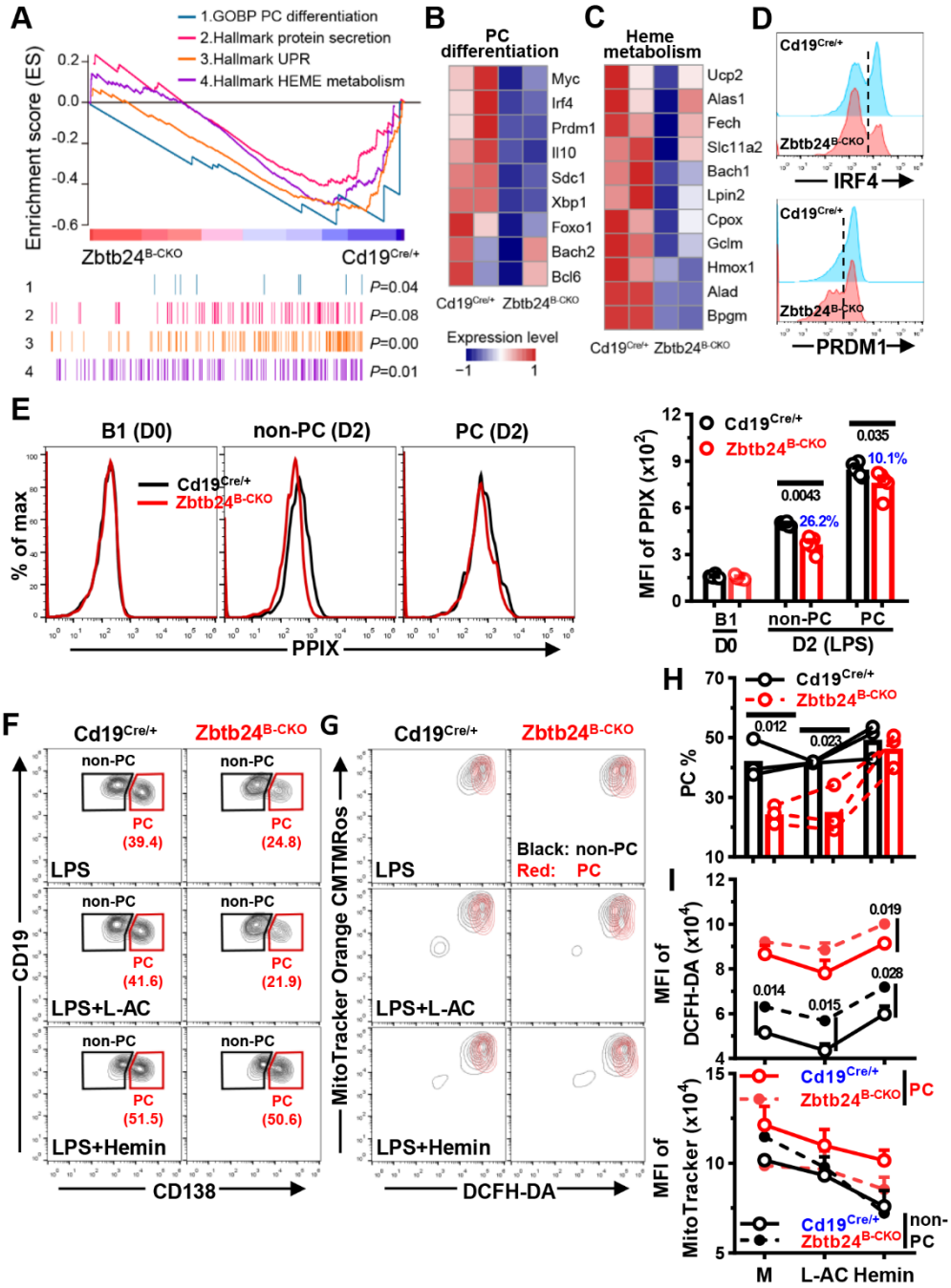

Figure 6. Zbtb24-deficiency blunts the differentiation of B1 cells into PCs through repressing the biosynthesis of heme. FACS-sorted peritoneal CD19^{+}B220^{low}CD23^{-} B1 cells were stimulated with 0.1 μg/ml LPS in 96-U bottom plate for 24 hrs (RNA-seq, **A-C**) or 2-3 days without/with additional L-AC (250 μM)/Hemin (25 μM) to induce PC differentiation (**D-I**). **A**, GSEA plots of genes involved in PC differentiation, protein secretion, unfolded protein response (UPR), and heme metabolism in LPS-stimulated Zbtb24$^{B\text{-}CKO}$ *vs.* Cd19$^{Cre/+}$ B1 cells. **B&C**, heatmaps showing the dysregulated genes regulating the differentiation of PC cells (**B**) or heme metabolism in cells (**C**) identified by RNA-seq analysis. The complete lists of enriched genes regulating UPR and heme metabolism were provided in Figure S10B. **D**, representative half-offset histograms showing the levels of intracellular IRF4 & PRDM1 on in LPS-stimulated B1 cells on D2. **E**, representative overlayed histograms (*left*) and cumulative data (*right*) showing the levels of intracellular PPIX in resting control *vs.* Zbtb24$^{B\text{-}CKO}$ B1 cells (D0) or gated CD138^{-} non-PC & CD138^{+} PC cells in LPS-stimulated cultures on D2. **F&H**, representative contour-plots (**F**) and bar graphs (**H**) showing the percentages of CD19^{low}CD138^{+} PCs in differentially cultured Cd19$^{Cre/+}$ *vs.* Zbtb24$^{B\text{-}CKO}$ B1 cells on day 3. **G**, representative overlayed contour-plots showing the intracellular ROS levels (visualized by DCFH-DA) and mitochondrial mass/membrane potentials (detected by MitoTracker Orange CMTMRos) in gated CD138^{-} non-PC (black) *vs.* CD138^{+} PC (red) cells in cultured B1 cells on day 3. **I**, bar graphs showing the ROS levels (MFI of DCFH-DA, top) or mitochondrial mass/membrane potential (MFI of MitoTracker, bottom) in gated non-PC/PC cells in Cd19$^{Cre/+}$ *vs.* Zbtb24$^{B\text{-}CKO}$ B1 cultures. Gates for CD138^{-} non-PC and CD138^{+} PC were illustrated in **F**. Each dot in **E&H** represents a single mouse of the indicated genotype (male, 12-14 weeks of age), while results in **I** are expressed as mean ± SEM (n=3). Numbers in **E**, **H &I** indicate *P* values determined by student *t*-test. Blue numbers in **E** denote percents of reduction.

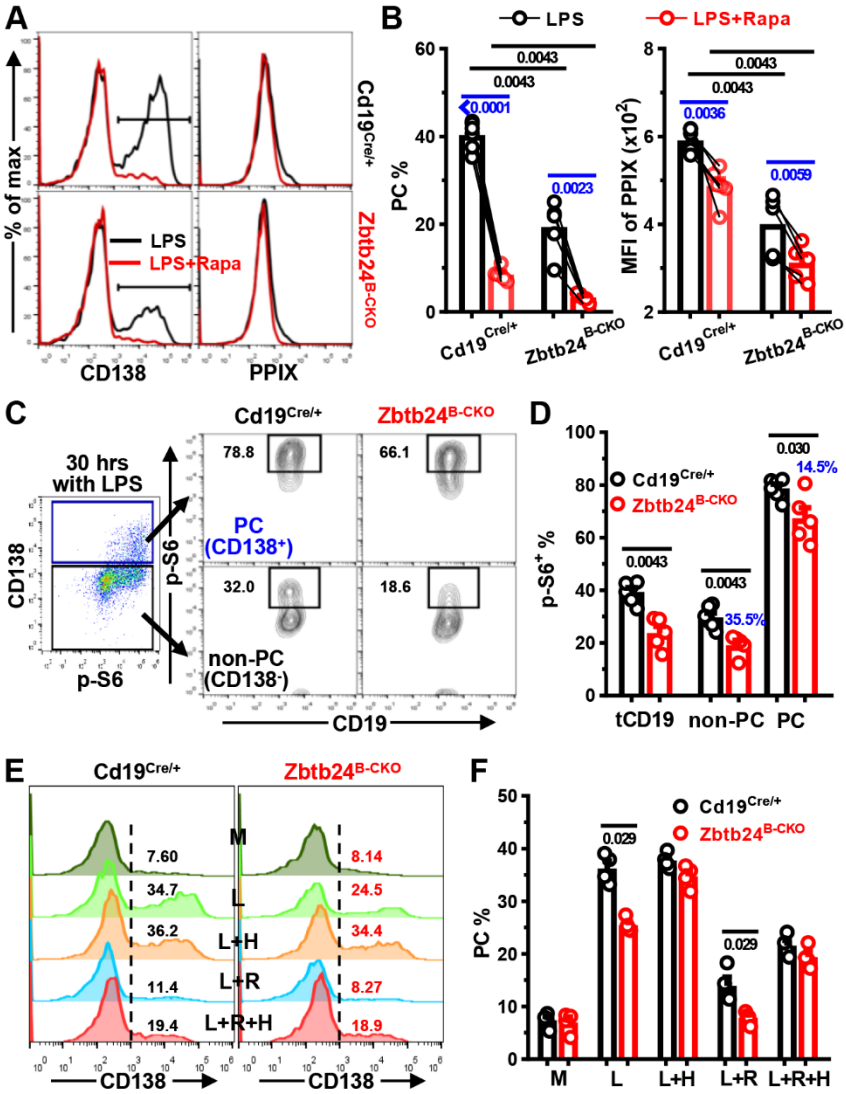

Figure 7. Zbtb24-ablation represses the mTORC1 activity, which promotes heme synthesis and PC differentiation of B1 cells. Peritoneal CD19^{+}B220^{low}CD23^{-} B1 cells were stimulated with 0.1 μg/ml LPS in the absence/presence of Rapamycin (Rapa, 10 nM) up for 2 days (**A-D**). **A&B**, representative overlayed histograms (**A**) and bar graphs (**B**) showing the PC differentiation (*left panel*) and PPIX expression (*right panel*) in B1 cells cultured with LPS ± Rapa on day 2. **C&D**, representative FACS-plots (**C**) and bar graphs (**D**) showing the expression of phosphorylated ribosomal protein S6 (p-S6) in gated CD138^{+} PC or CD138^{-} non-PC cells derived from Cd19$^{Cre/+}$/Zbtb24^{B-CKO} B1 cells after stimulation with LPS for 30 hrs. tCD19 denotes total CD19^{+} B cells and blue numbers indicate percent of reduction in gated Zbtb24^{B-CKO} populations compared to the corresponding control counterparts (**D**). **E&F**, representative histograms (**E**) and bar graphs (**F**) showing the PC differentiation of B1 cells cultured in medium (M), LPS (L), and LPS plus Hemin (25 μM, L+H), Rapamycin (10 nM, L+R) or both (L+R+H) for 2 days. Each dot represents a single mouse of the indicated genotype (12-week males in **A-D**, and 9-week females in **E&F**). Black/blue numbers below horizonal lines indicate *P* values determined by Mann-Whitney test or paired *t*-test, respectively.

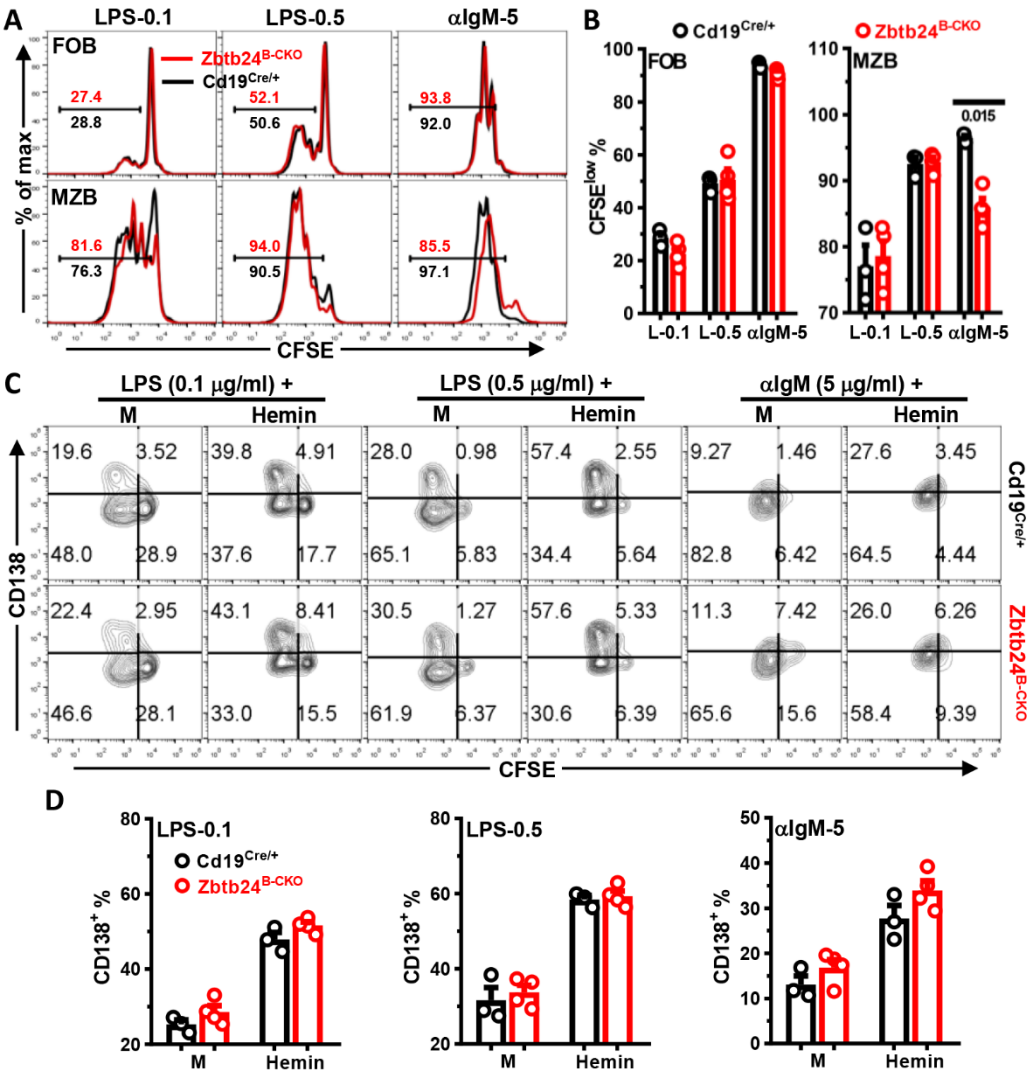

Figure 8. Zbtb24-deficiency has no effect on the differentiation, but slightly reduces BCR-triggered proliferation of MZB cells *in vitro*. $CD19^{+}CD23^{high}CD21^{low}$ FOB and $CD19^{+}CD23^{low}CD21^{high}$ MZB cells were FACS-sorted from spleens of $Cd19^{Cre/+}$ & $Zbtb24^{B\text{-}CKO}$ mice (male, 14 weeks old), labeled with CFSE (10 μM), and then cultured (~1 x 10^5 cells/well in 96-U bottom plate) with LPS (0.1/0.5 μg/ml), αIgM (5 μg/ml) in the absence/presence of exogenous Hemin (25 μM). On day 3, cells were collected, stained with anti-CD138 before flow cytometry analysis. **A**, representative overlayed histograms showing the cell division profiles (CFSE) of cultured control *vs.* $zbtb24^{B\text{-}CKO}$ FOB (top) and MZB (bottom) cells. Numbers indicate the percentages of divided $CFSE^{low}$ cells. **B**, bar graphs showing the percentages of divided $CFSE^{low}$ cells in cultured FOB and MZB cells. **C**, representative contour-plots showing the proliferation (CFSE) *vs.* differentiation (CD138) of splenic control (top) *vs.* $zbtb24^{B\text{-}CKO}$ (bottom) MZB cells in different cultures. **D**, bar graphs showing the percentages $CD138^{+}$ PC cells in differently stimulated MZB cells purified from control *vs.* $zbtb24^{B\text{-}CKO}$ mice. Each symbol represents a single mouse of the indicated genotype, and numbers below horizonal lines in **B** indicate *P* values determined by student *t*- test.

Table S2. gRNA and primer sequences used in this study.

Name	Sequence (5'→3')	Application
Zbtb24-gRNA1	CCGGAGGGCCGTACAGACTTTTG	loxp1 insertion
Zbtb24-gRNA2	CCAGCCTCACGTAGACACTTTAT	loxp2 insertion
Zbtb24-screen F2	TAACGGACCGGAGGGCGTCG	ES clone selection
Zbtb24-screen R3	TCAAGTGATAAAGTGTCTACGTGAGGTGCTA	ES clone selection
Zbtb24-WT Fw	CCATCTTGTAAATATCTTCTGGGTGTCT (in WT allele)	Genotyping (Zbtb24)
Zbtb24-WT Rv	GATAAAGTGTCTACGTGAGGCTGGG (in WT allele)	Genotyping (Zbtb24)
Zbtb24-CKO Rv	GTGTCTACGTGAGGTGCTATAACTTCG (in loxp allele)	Genotyping (Zbtb24)
Cd19-Cre-M Fw	GCGGTCTGGCAGTAAAAACTATC (in Cre allele)	Genotyping (Cd19-Cre)
Cd19-Cre-M Rv	GTGAAACAGCATTGCTGTCACTT (in Cre allele)	Genotyping (Cd19-Cre)
Cd19-Cre-W Fw	CCTCTCCCTGTCTCCTTCCT (in WT allele)	Genotyping (Cd19-Cre)
Cd19-Cre-W Rv	TGGTCTGAGACATTGACAATCA (in WT allele)	Genotyping (Cd19-Cre)
mZbtb24 Fw	CCTTGTGGGCAGCTTATGGT	RT-qPCR (Zbtb24)
mZbtb24 Rv	CAAGGCTTTATGGGCTCGGA	RT-qPCR (Zbtb24)
mGapdh Fw	AACTTTGGCATTGTGGAAGG	RT-qPCR (Gapdh)
mGapdh Rv	GGATGCAGGGATGATGTTCT	RT-qPCR (Gapdh)

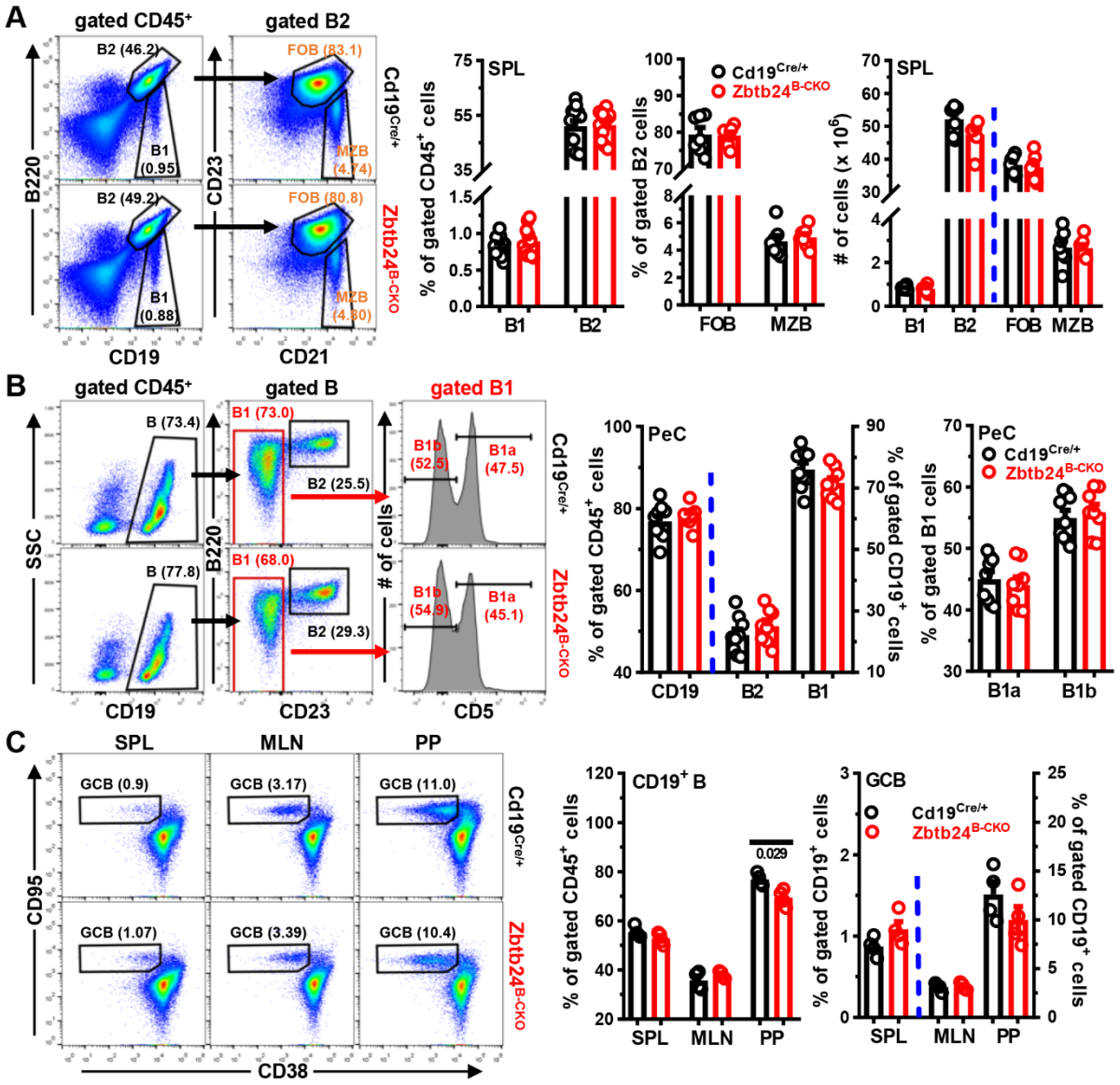

Figure S1. Little impact of Zbtb24-deficiency on the phenotype of B cells in the periphery of mice. Cells from the spleens (SPL), peritoneal cavities (PeC), mesenteric lymph nodes (MLN) and Peyer's patches (PP) of mice (female, 8-10 weeks old) were stained with antibodies against the indicated surface molecules before flow cytometry analyses. **A&B**, representative pictures/bar graphs showing the gating strategies/percentages of B2 ($CD19^{+}B220^{high}$ in SPL or $CD19^{+}B220^{high}CD23^{+}$ in PeC, respectively), B1 ($CD19^{+}B220^{low}$ in SPL or $CD19^{+}B220^{low}CD23^{-}$ in PeC, respectively), B1a/b ($CD5^{+}/CD5^{-}$, respectively, within gated B1), follicular (FOB)/marginzal zone (MZB) ($CD23^{high}CD21^{low}/CD23^{low}CD21^{high}$, repectively, within gated B2) in the SPL (**A**) or PeC (**B**) of $Cd19^{Cre/+}$ and $Zbtb24^{B\text{-}CKO}$ mice. The absolute cell numbers are also shown in the far-right panel of **A**. **C**, representative pseudo-plots/bar graphs showing the gating strategies/percentages of germinal center B (GCB, $CD95^{high}CD38^{low}$) within gated $CD19^{+}$ B cells in the SPL, MLN and PP of $Cd19^{Cre/+}$ & $Zbtb24^{B\text{-}CKO}$ mice. Each symbol represents a single mouse of the indicated genotype. The absolute numbers of indicated B-cell subsets did not differ significantly in the PeC, MLN and PP of the two groups of mice (data not shown). AU, arbitrary units. Pooled data from two-independent experiments were shown in **A&B**.

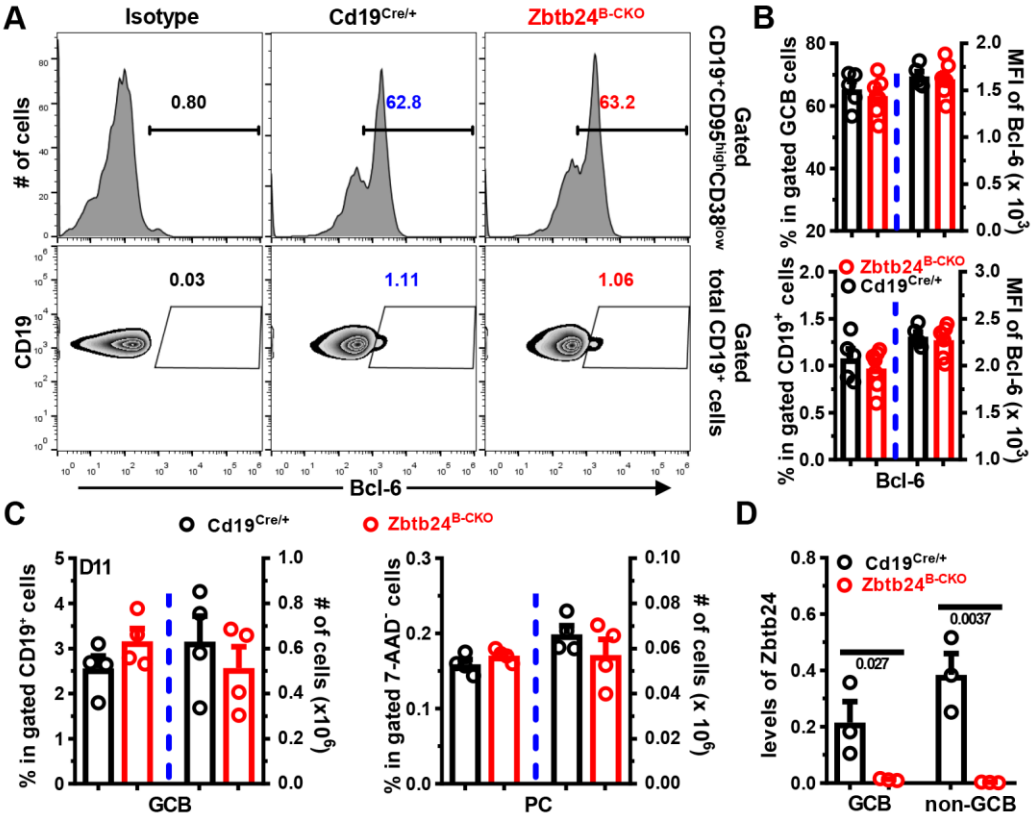

Figure S2. No effect of Zbtb24-deficiency on the phenotype and number of GCB cells after TD-Ag immunization. Splenic cells in mice were stained with antibodies against CD19/CD95/CD38 & Bcl-6 (intracellular) or CD19/CD138 plus 7-AAD to visualize the percents/phenotypes of GCB or PC cells in mice depicted in Figure 2A-C on D14 post NP_{19}-OVA/IFA immunization (**A&B**) or on D11 post i.p. immunization with sheep red blood cells (SRBC, $1x10^9$ cells/200 µl PBS/mouse, female, 8 weeks of age) (**C&D**). **A**, representative histograms (*upper panel*) or zebra-plots (*lower panel*) showing the percentages of $Bcl6^+$ cells in gated $CD19^+CD95^{high}CD38^{low}$ GCB cells (*upper panel*) or total $CD19^+$ B cells (*lower panel*) in control $Cd19^{Cre/+}$ and $Zbtb24^{B\text{-}CKO}$ mice. **B**, bar graphs showing the percentages of $Bcl6^+$ cells/MFI of Bcl6 in gated $CD19^+CD95^{high}CD38^{low}$ GCB cells (*upper panel*) or total $CD19^+$ B cells (*lower panel*). **C**, bar graphs showing the percentages/absolute numbers of $CD19^+CD95^{high}CD38^{low}$ GCB and $CD19^{low}CD138^{high}$ PC cells in spleens of mice on D11 post immunization. **D**, mRNA levels of Zbtb24 in FACS-purified $CD19^+CD95^{high}CD38^{low}$ GCB and $CD19^+CD95^-CD38^+$ non-GCB cells from spleens of immunized mice. Each symbol represents a single mouse of the indicated genotype, and numbers below horizon lines indicate *P* values determined by student *t*-test.

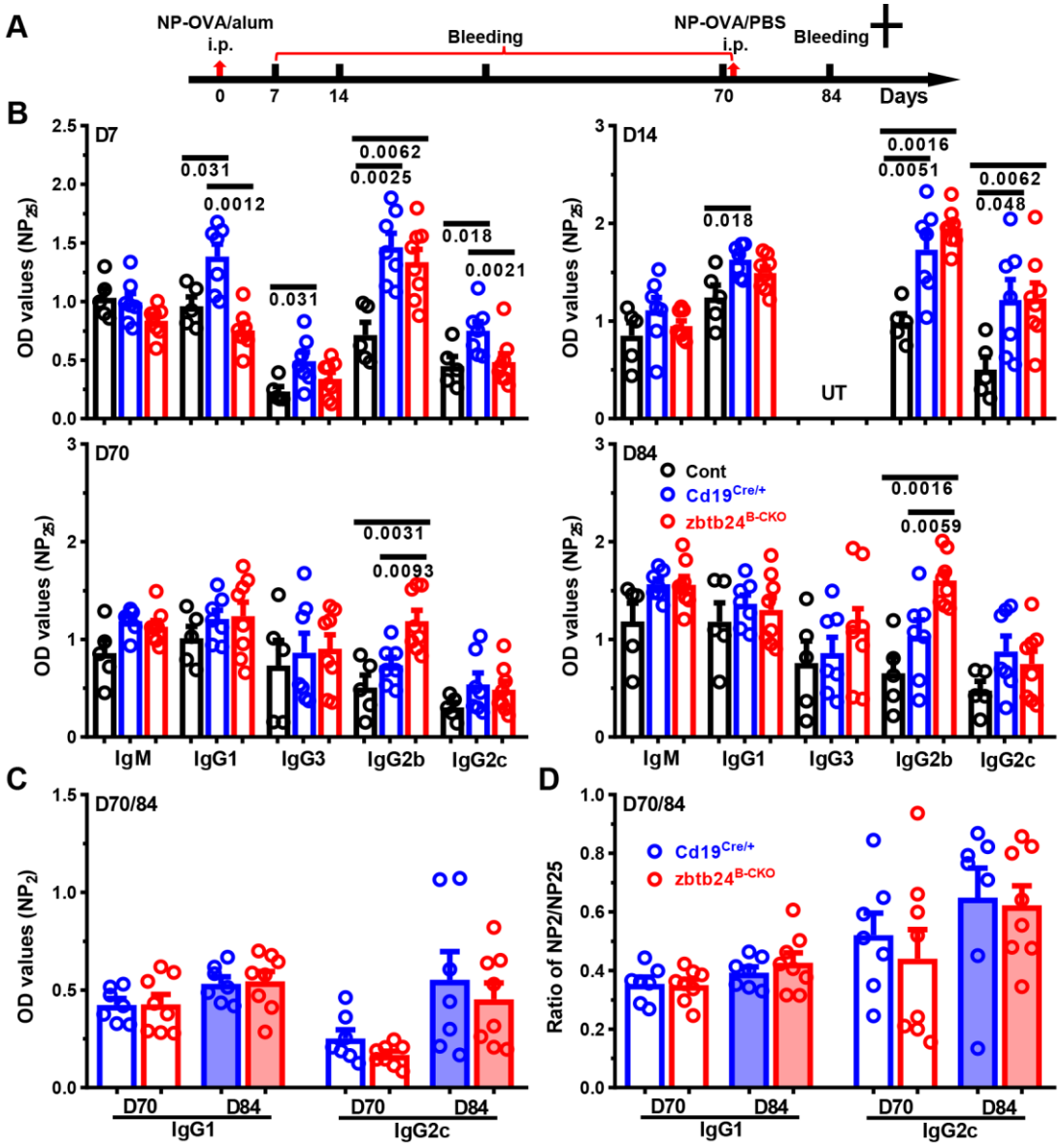

Figure S3. Deficiency of Zbtb24 in B cells has no impact on the long-term antibody responses in mice after NP_{19}-OVA/alum immunization. Mice (female, 8 weeks of age) were i.p. immunized with alum-precipitated NP_{19}-OVA (NP-OVA/alum, 100 μg/100 μl/mouse) on D0, and rechallenged with NP_{19}-OVA in PBS (50 μg/100 μl/mouse) on D70. **A**, a schematic diagram depicting the experimental setup. **B&C**, bar graphs showing the optical density (OD) values of NP-specific antibody subtypes against coated NP_{25}-BSA (NP_{25}, **B**) or NP_2-BSA (NP_2, **C**) in diluted sera of $Zbtb24^{loxp/loxp}$ (Cont), $Cd19^{Cre/+}$ and $Zbtb24^{B\text{-}CKO}$ mice on indicated days. **D**, bar graphs showing the ratios of relatively high-affinity (NP_2) to low-affinity (NP_{25}) NP-specific IgG1 & IgG2c in $Cd19^{Cre/+}$ and $Zbtb24^{B\text{-}CKO}$ mice on D70 & D84. Each dot represents a single mouse of the indicated genotype and numbers below horizonal lines indicate *P* values determined by Mann-Whitney test. UT, untested.

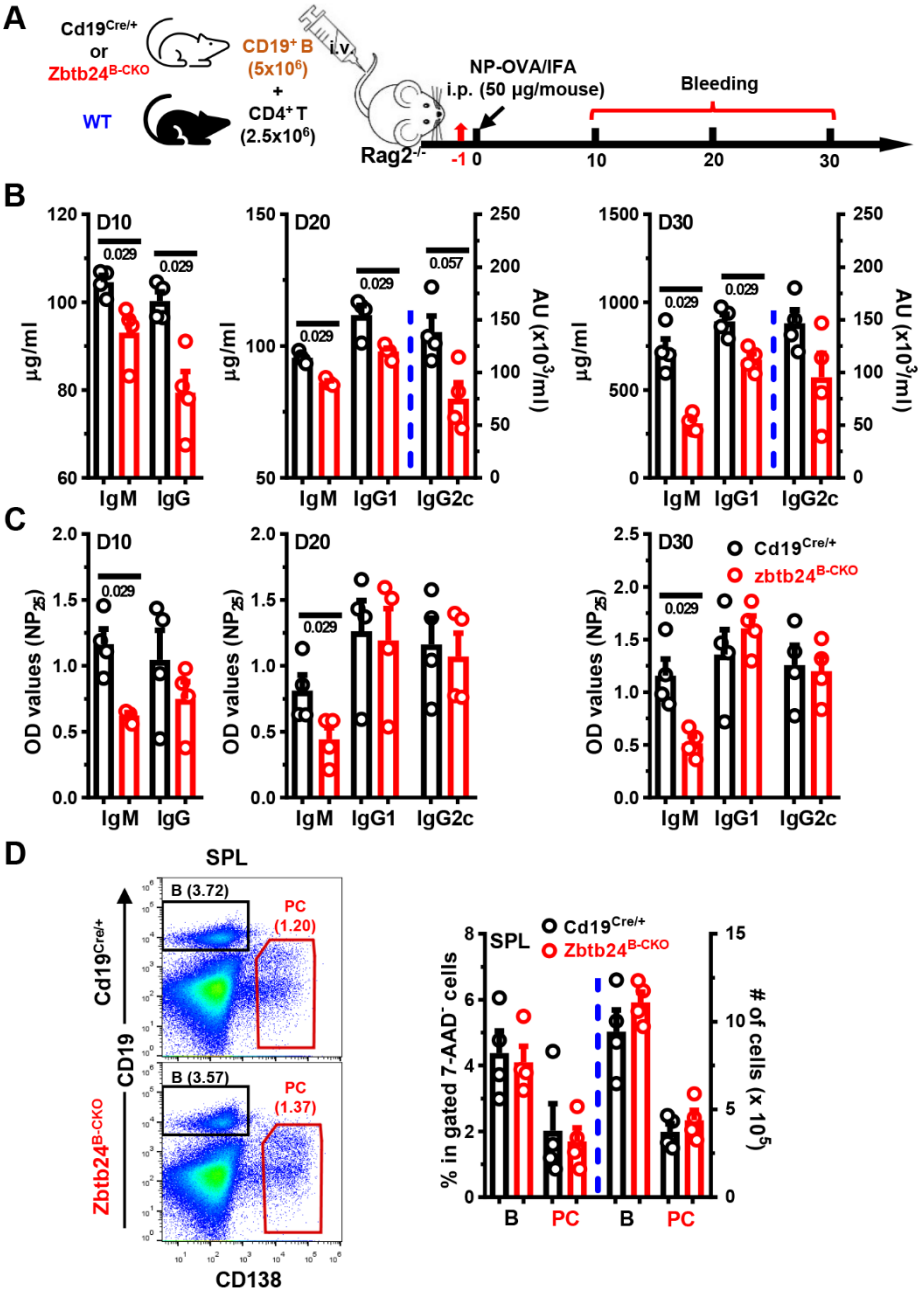

Figure S4. Reduced total antibody-producing ability of Zbtb24$^{B\text{-}CKO}$ splenic B cells after adoptive transfer. CD19^{+} B cells, enriched from Zbtb24$^{B\text{-}CKO}$ or control Cd19$^{Cre/+}$ mice (male, 8 weeks of age) by magnetic beads, were mixed with CD4^{+} T cells (purified from male WT mice) at the ratio of 2:1 before being intravenously (i.v.) injected into the Rag2$^{-/-}$ recipient mice (5x10^{6} B cells plus 2.5x10^{6} T cells per mouse). One day later, recipient mice were immunized with NP$_{19}$-OVA emulsified in IFA (NP-OVA/IFA) intraperitoneally (i.p.). Blood was taken at indicated times, and total or NP-specific antibody levels in sera were determined by ELISA. **A**, a schematic flow-chart of the experiment setup. **B&C**, bar graphs showing levels of total (**B**) or NP-specific (**C**) IgM/IgG or IgG1/IgG2c levels in sera of recipient mice at indicated times. **E**, bar graphs showing the percentages and absolute numbers of CD19^{+} B cells or CD19$^{-/low}$CD138^{+} plasma cells (PC) in the spleens (SPL) and bone marrows (BM) of Cd19$^{Cre/+}$ *vs.* Zbtb24$^{B\text{-}CKO}$ mice. Representative pseudo-plots showing the gates for each population were shown in **D**. Each dot represents a single recipient mouse, and numbers below horizontal lines indicate *P* values. AU, arbitrary units.

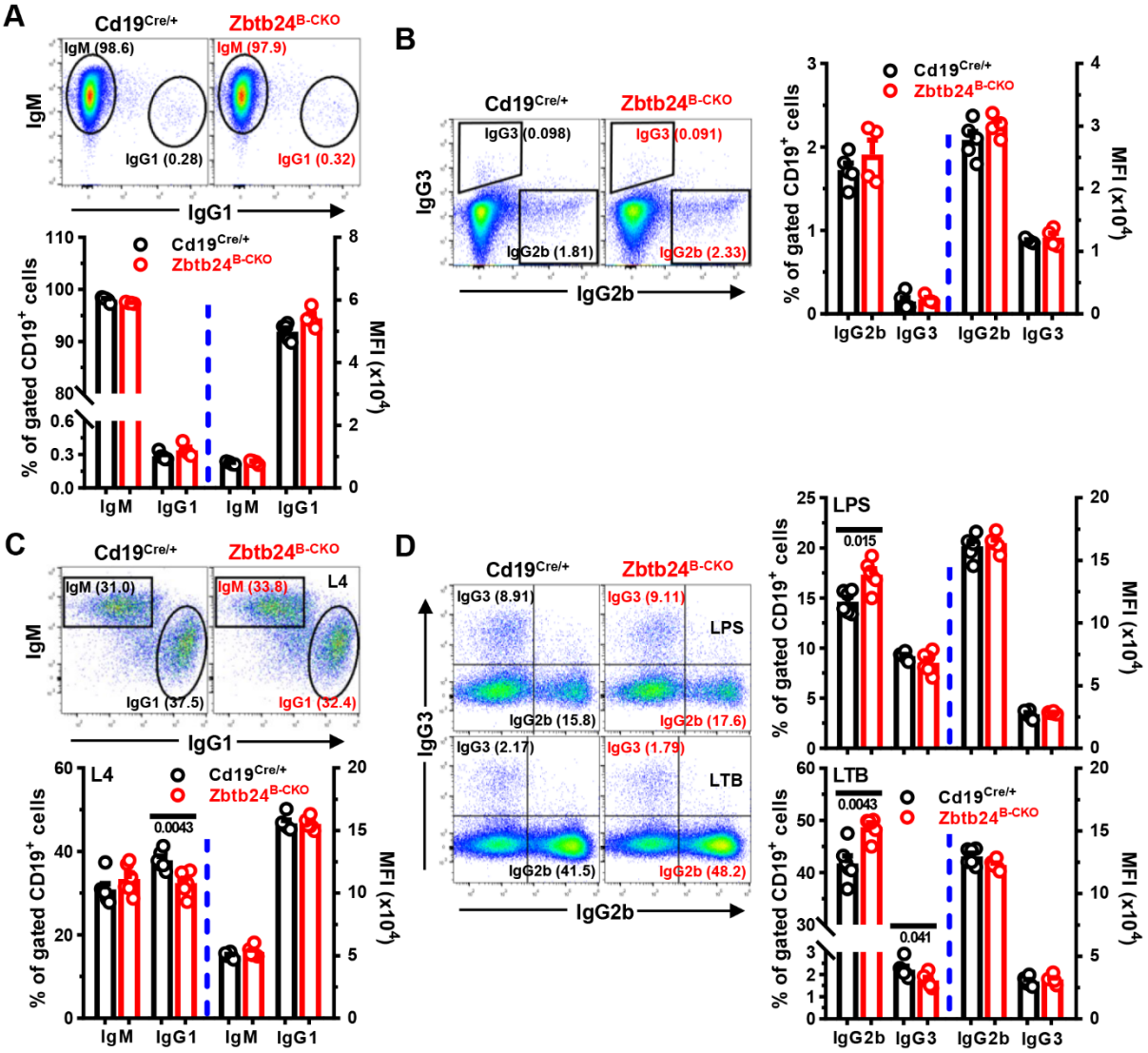

Figure S5. Grossly intact CSR abiltiy of Zbtb24$^{B\text{-}CKO}$ B cells. Splenic B cells (2 x 10^5 cells/well) from Cd19$^{Cre/+}$ or Zbtb24$^{B\text{-}CKO}$ mice were stimulated with LPS (10 μg/mL) in the absence/presence of IL-4 (25 ng/ml) or TGF-β (1 ng/ml) plus BAFF (10 ng/ml) in 96 U-bottom plates. On day 4, cells were collected and expressions of surface IgM/IgG2b/IgG3 & IgG1 on B cells were analyzed by flow cytometry. **A&C,** representative pseudo-plots and bar graphs showing the surface IgM/IgG1 on B cells before (**A**) and after culture with LPS plus IL-4 (L4, **C**). **B&D**, representative pseudo-plots/bar graphs showing the surface IgG2b/IgG3 on B cells before (**B**) and after culture with LPS without (*upper panel* in **D**)/with TGF-β & BAFF (LTB, *lower panel* in **D**). Each symbol represents a single mouse of the indicated genotype (female, 10 weeks of age), and numbers below horizontal lines indicate *P* values. MFI, mean fluorescence intensity.

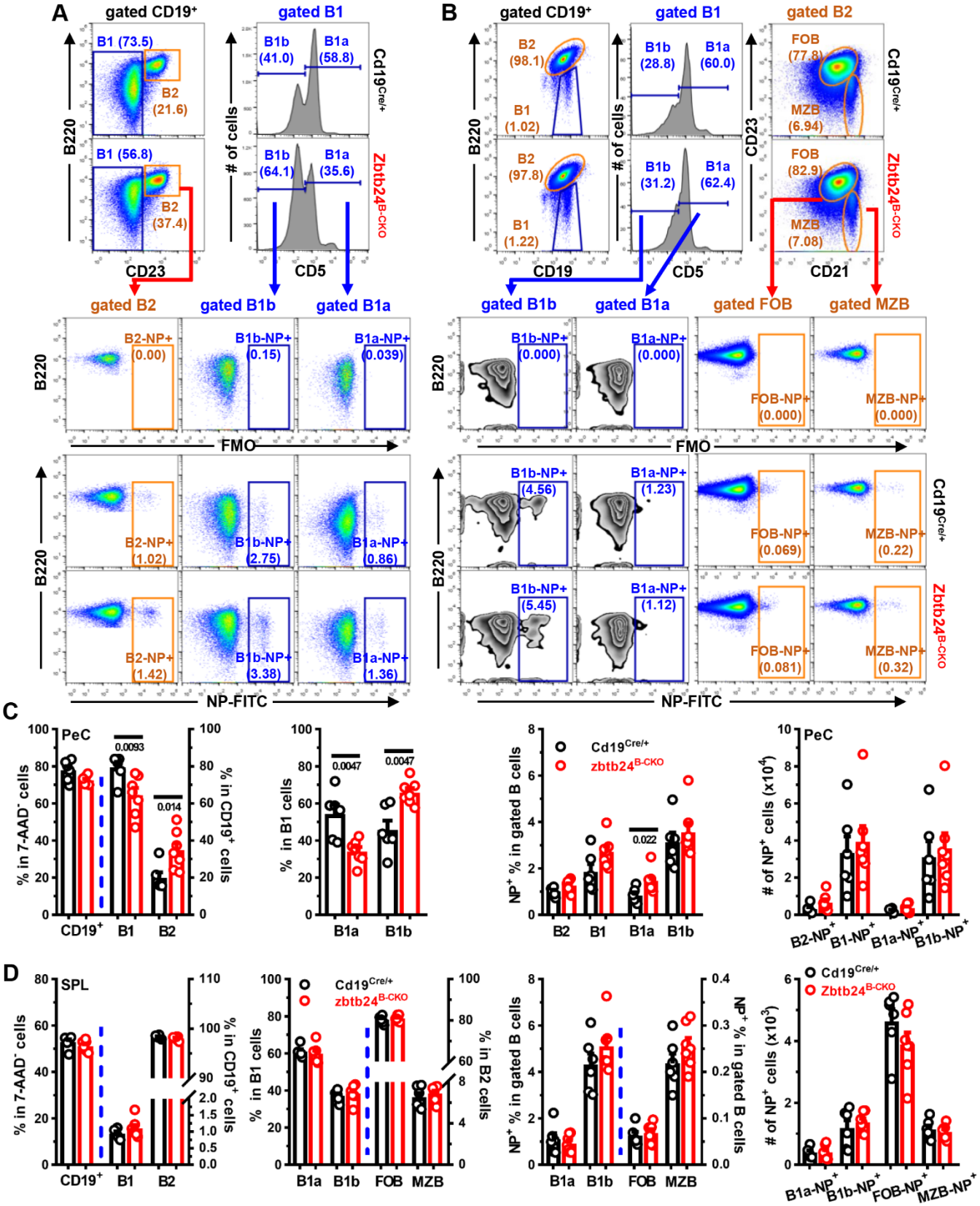

Figure S6. Comparable numbers of NP$^+$ B cells in Cd19$^{Cre/+}$ & Zbtb24$^{B\text{-}CKO}$ mice on D35 after NP-Ficoll immunization. Peritoneal and splenic cells in NP-Ficoll immunized mice (depicted in Figure 3A-E) were stained with antibodies against B220/CD19/CD5/CD21/CD23 in combination with 7-AAD and NP-FITC. **A&B**, representative flow cytometry plots showing the gating strategies to identify NP$^+$ cells within gated B2/B1, B1a/B1b & follicular (FOB)/marginal zone (MZB) B cells in peritoneal cavities (**A**) and spleens (**B**). Gates for NP$^+$ cells within B2 (B2-NP+), B1b (B1b-NP+), B1a (B1a-NP+), FOB (FOB-NP+) & MZB (MZB-NP+) were set based on the FMO (fluorescence minus one/FITC-channel) samples. **C&D**, bar graphs showing the percentages/absolute numbers of NP$^+$ cells within indicated B-cell subsets in peritoneal cavities (PeC, **C**) and spleens (SPL, **D**) of Cd19$^{Cre/+}$ & Zbtb24$^{B\text{-}CKO}$ mice. Each dot represents a single mouse of the indicated genotype, and numbers below horizonal lines indicate *P* values.

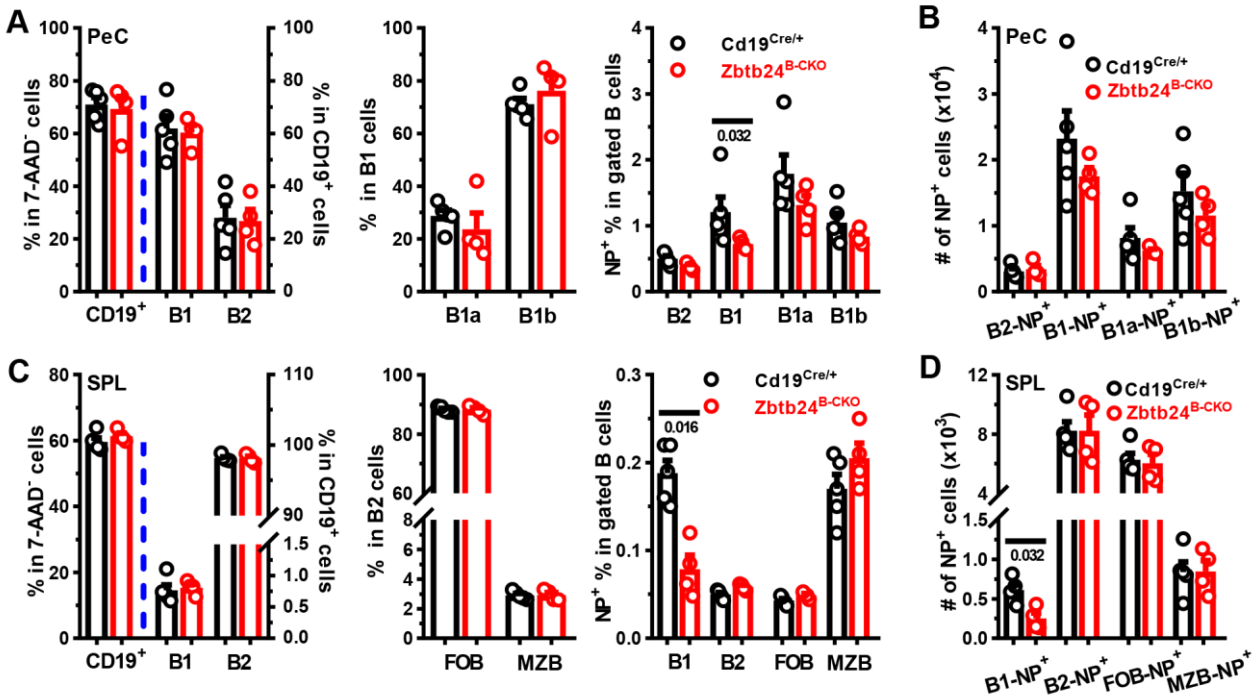

Figure S7. Reduced numbers of NP⁺ B1 cells in Zbtb24$^{B\text{-}CKO}$ mice after NP-LPS immunization. Peritoneal and splenic cells in NP-LPS immunized mice (depicted in Figure 3F-H) were stained and analyzed as described in Figure S6A&B. **A&B**, bar graphs showing the percentages (**A**) and absolute numbers (**B**) of NP⁺ cells within indicated B-cell subsets in peritoneal cavities (PeC) of mice. **C&D**, bar graphs showing the percentages (**C**) and absolute numbers (**D**) of NP⁺ cells within indicated B-cell compartments in spleens (SPL) of Cd19$^{Cre/+}$ *vs.* Zbtb24$^{B\text{-}CKO}$ mice. Each dot represents a single mouse of the indicated genotype, and numbers below horizonal lines indicate *P* values.

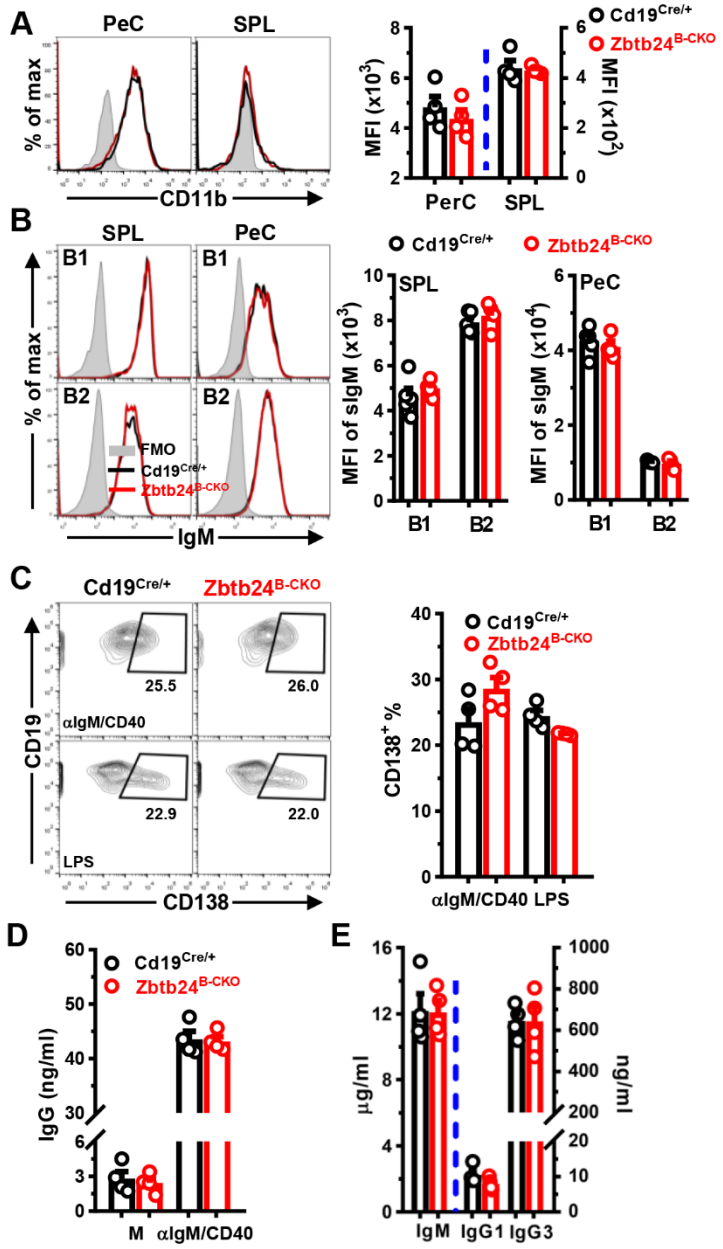

Figure S8. Zbtb24-deficiency has no impact on the differentiation and antibody-producing ability of splenic B cells *in vitro*. A&B, representative overlayed-histograms & bar graphs showing levels of surface CD11b (**A**) or IgM (sIgM, **B**) on splenic (SPL)/peritoneal (PeC) B1/B2 cells in Cd19$^{Cre/+}$ *vs.* Zbtb24$^{B\text{-}CKO}$ mice. Splenic and peritoneal cells were stained with antibodies against CD19/B220/CD23 & CD11b/IgM before flow cytometry analyses. **C**, representative contour-plots & bar graphs showing percentages of CD138^{+} PC cells in cultured splenic CD19^{+} B cells. **D&E**, levels of IgG (**D**) or IgM/IgG1/IgG3 (**E**) in supernatants of splenic B cells cultured in M, αIgM/CD40 (**D**) or LPS (**E**). CD19^{+} B cells were FACS-sorted from spleens of Cd19$^{Cre/+}$ & Zbtb24$^{B\text{-}CKO}$ mice, and subsequently cultured (1 x 10^5 cells/well in 96-well plate) in medium (M), anti-IgM & anti-CD40 (αIgM/CD40, 5/5 μg/ml) or LPS (10 μg/ml). On day 4, surface expressions of CD138 on cultured B cells were analyzed by flow cytometry, and antibody levels in culture supernatants were determined by ELISA (**C-E**). Each symbol represents a single mouse of the indicated genotype (female, 8-10 weeks of age).

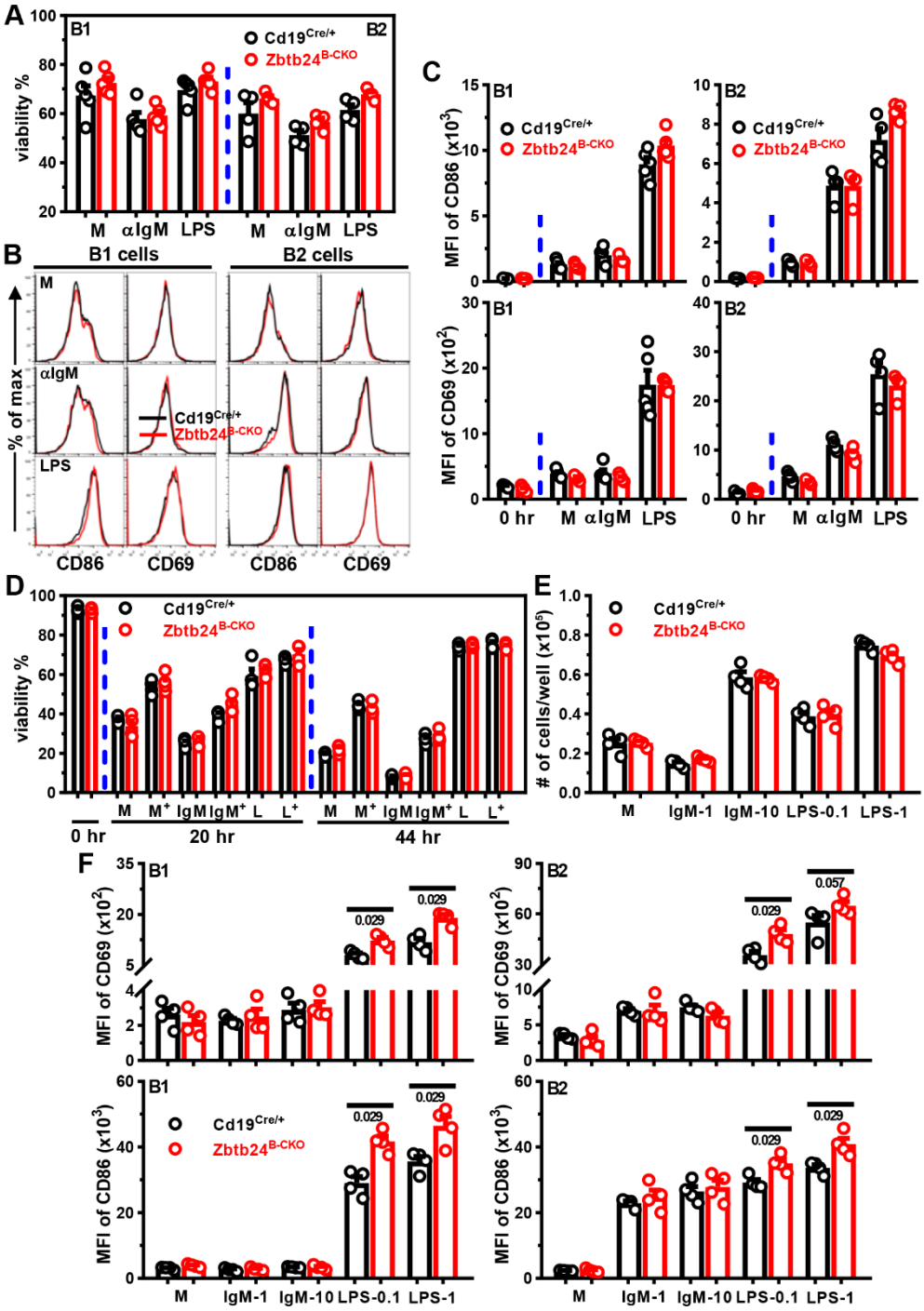

Figure S9. Zbtb24-deficiency does not compromise the survival, activation and proliferation of Zbtb24$^{B\text{-}CKO}$ B cells *in vitro*. CD19^{+}B220^{low}CD23^{-} B1 and CD19^{+}B220^{high}CD23^{+} B2 cells were FACS-sorted from peritoneal cavities of Cd19$^{Cre/+}$ & Zbtb24$^{B\text{-}CKO}$ mice, and subsequently cultured (2-5 x 10^4 cells/well in 96-U bottom plate) in medium (M), αIgM (2 μg/ml) or LPS (0.5 μg/ml). Viabilities (based on forward/side scatter) and surface levels of CD69/CD86 were analyzed by flow cytometry (**A-C**). **A**, bar graphs showing viabilities of peritoneal B1 & B2 cells at 24 hrs. **B&C**, representative overlayed histograms (**B**) or bar graphs (**C**) showing surface expressions of CD86 & CD69 on 24-hr cultured peritoneal B1/B2 cells derived from Cd19$^{Cre/+}$ *vs.* Zbtb24$^{B\text{-}CKO}$ mice before (0 hr) and after 24 hr's culture. CD19^{+} B cells were purified from spleens of Cd19$^{Cre/+}$ & Zbtb24$^{B\text{-}CKO}$ mice, and subsequently cultured (1.5-2 x 10^5 cells/well in 96-well plate) in medium, anti-IgM or LPS before flow cytometry analysis (**D-F**). **D**, bar graphs showing the percents of living cells (7-AAD^{-} & Annexin V^{-}) before (0 hr) or after cultures in M, 1 μg/ml anti-IgM (IgM) or LPS (L) in the absence/presence of 0.2 μg/ml BAFF (indicated by a '+' in the upper-right corner) for 20 & 44 hrs. **E**, bar graphs showing the numbers of living cells (based on forward/side scatter) in different cultures on day 3. **F**, bar graphs showing the expression levels of surface CD69 (top row) and CD86 (bottom row) on gated B2 (CD19^{+}B220^{high}, left column) or B1 (CD19^{+}B220^{low}, right column) cells after 20 hrs' culture in medium (M), 1/10 μg/ml anti-IgM (IgM-1/IgM-10, respectively), 0.1/1 μg/ml LPS (LPS-0.1/LPS-1, respectively). Each symbol represents a single mouse of the indicated genotype (12-week-old males in **A-C**, and 8-week-old females in **D-F**), and numbers below horizontal lines in **F** indicate *P* values.

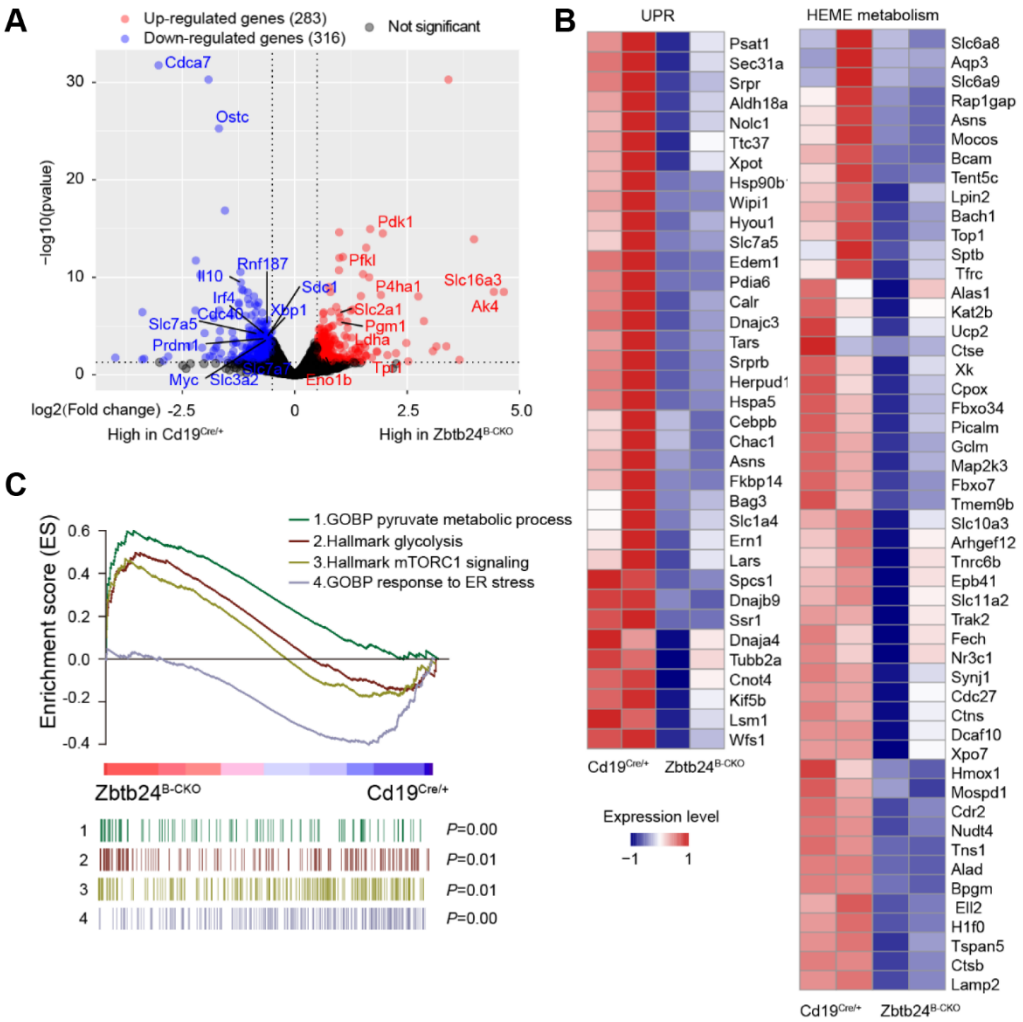

Figure S10. Dysregulated genes/signaling pathways in Zbtb24-deficient B1 cells. FACS-sorted peritoneal $CD19^{+}B220^{low}CD23^{-}$ B1 cells were stimulated with 0.1 μg/ml LPS in 96-U bottom plate for 24 hrs (related to Figure 6A-C). **A**, volcano plots showing upregulated (red) or downregulated (blue) genes in $Zbtb24^{B\text{-}CKO}$ B1 cells. **B**, heatmaps showing the enriched genes affiliated to UPR and heme metabolism in Zbtb24-deficient B1 cells by GSEA. **C**, GSEA plots showing the enrichment of genes regulating pyruvate metabolism, glycolysis, mTORC1 signaling and ER stress in LPS-stimulated $Zbtb24^{B\text{-}CKO}$ *vs.* $Cd19^{Cre/+}$ B1 cells.

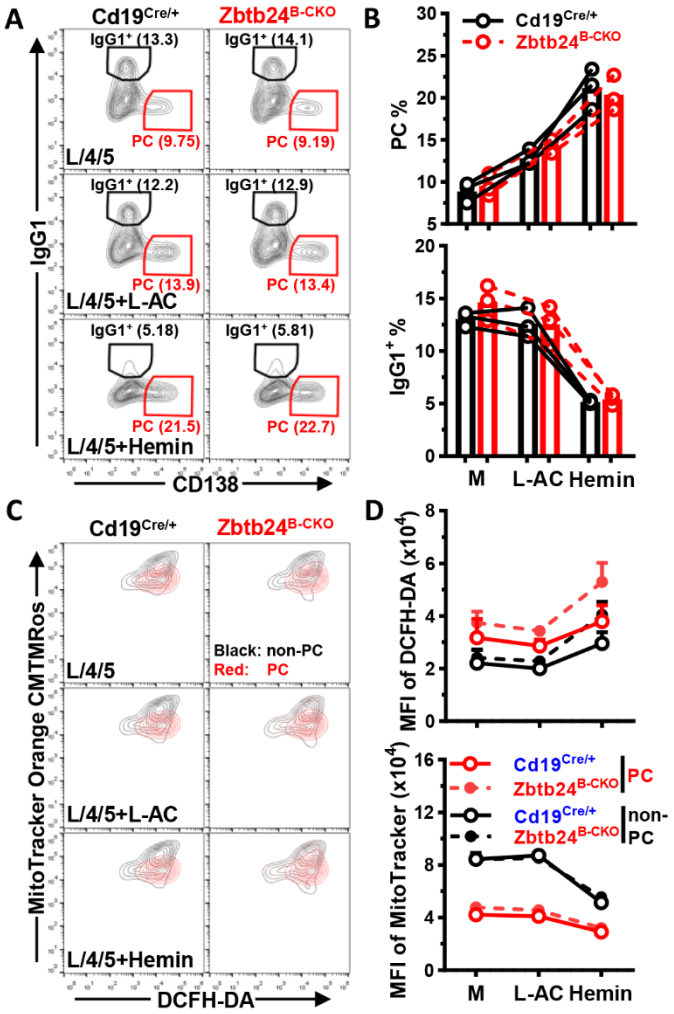

Figure S11. No effect of Zbtb24-deficiency on heme metabolism in stimulated splenic B cells. Splenic B cells, isolated from Cd19$^{Cre/+}$ or Zbtb24$^{B\text{-}CKO}$ mice, were stimulated with 10 µg/ml LPS plus 10 ng/ml IL-4 & IL-5 (L/4/5) without/with additional L-AC (250 µM) or Hemin (25 µM) in 96-U bottom plate for 4 days. **A&B**, representative contour-plots (**A**) and bar graphs (**B**) showing the percentages of class-switched CD138^{-}IgG1^{+} B cells (IgG1^{+}) or differentiated IgG1^{-}CD138^{+} PC in stimulated Cd19$^{Cre/+}$ *vs.* Zbtb24$^{B\text{-}CKO}$ splenic B cells on day 4. **C**, representative overlayed contour-plots showing the intracellular ROS levels (visualized by DCFH-DA) and mitochondrial mass/membrane potentials (detected by MitoTracker Orange CMTMRos) in gated CD138^{-} non-PC (black) *vs.* CD138^{+} PC (red) in cultured splenic B cells on day 4. **D**, line graphs showing the ROS levels (MFI of DCFH-DA, *upper panel*) and mitochondrial mass/membrane potential (MFI of MitoTracker, *lower panel*) in gated non-PC/PC cells in Cd19$^{Cre/+}$ *vs.* Zbtb24$^{B\text{-}CKO}$ splenic B cell cultures. Each dot in **B** represents a single mouse of the indicated genotype (male, 14 weeks of age), while results in **D** are expressed as mean ± SEM (n=3).